Global force-torque phase diagram for the DNA double helix:
Structural transitions, triple points, and collapsed plectonemes

John F. Marko

Department of Physics and Astronomy and Department of Molecular Biosciences, Northwestern University, Evanston, Illinois 60208, USA

Sébastien Neukirch

CNRS, UMR 7190, Institut Jean Le Rond d'Alembert, F-75005 Paris, France
and UPMC Université Paris 06, UMR 7190, Institut Jean Le Rond d'Alembert, F-75005 Paris, France

We present a free energy model for structural transitions of the DNA double helix driven by tensile and torsional stress. Our model is coarse grained and is based on semiflexible polymer descriptions of B-DNA, underwound L-DNA, and highly overwound P-DNA. The statistical-mechanical model of plectonemic supercoiling previously developed for B-DNA is applied to semiflexible polymer models of P- and L-DNA to obtain a model of DNA structural transitions in quantitative accord with experiment. We identify two distinct plectonemic states, one "inflated" by electrostatic repulsion and thermal fluctuations and the other "collapsed," with the two double helices inside the supercoils driven to close contact. We find that supercoiled B and L are stable only in the inflated form, while supercoiled P is always collapsed. We also predict the behavior and experimental signatures of highly underwound "Q"-DNA, the left-handed analog of P-DNA; as for P, supercoiled Q is always collapsed. Overstretched "S"-DNA and strand-separated "stress-melted" DNA are also included in our model, allowing prediction of a global phase diagram for forces up to 1000 pN and torques between ±60 pN nm, or, in terms of linking number density, from $\sigma = -5$ to $+3$.

I. INTRODUCTION

Relaxed double-stranded DNA (dsDNA) in physiological aqueous solution (pH 7.5, 150 mM univalent ion concentration, 25 to 40 °C) is found in the double helix B form, with a right-handed helical repeat of $n_B = 10.5$ base pairs (bp) (helix rotation angle $\psi_B = 2\pi/n_B = 0.60$ radians per base pair) and a contour length of $a_B = 0.34$ nm per base pair (nm/bp). The B form is stabilized by hydrogen bonding between complementary bases on the two strands and hydrophobic stacking interactions between adjacent bases on each strand. Relatively small variations of the basic B structure occur with varied base sequence, making B-DNA described well at mesoscopic scales as a semiflexible polymer with a persistence length of $A \approx 50$ nm [1]. An example of the utility of this coarse-grained description is its ability to describe polymer stretching elasticity of B-DNA under forces up to ≈10 pN [2]. Addition of harmonic twisting elasticity allows supercoiling, the wrapping of the molecule around itself in response to sufficient torsional stress, to be quantitatively described [3–9].

This simple picture of B-DNA quickly breaks down when one considers situations where the double helix is put under large tensile or torsional stress. Such situations include highly constrained bending or twisting, as occur during cyclization experiments on short DNAs or in other situations where strong local constraints are put on the double helix to force local elastic failure (e.g., kinks or local regions of DNA denaturation) [10,11]. Alternately, one might drive structural reorganization of dsDNA by applying sufficient static torsional or tensile stresses. The soft (noncovalently bonded) nature of the base-pairing and stacking interactions combined with the strong, covalently bonded backbones with plenty of stored length in the B form (the backbones have a contour length approximately twice as long as that of the B form) suggest that a wide range of possible reorganizations of the double helix might be possible.

The most basic reorganization of B-DNA is separation of the two strands from one another. Strand separation has long been studied using thermal "melting" of dsDNA, which occurs at temperatures ranging from 50 to 80°C depending on base-pair composition. Such experiments provide data for the free energy difference per base pair ϵ_M between B and single-stranded DNA, as a function of sequence. Given the sequence-averaged value of $\epsilon_M \approx 2.5 k_B T$/bp one can anticipate that when under force of roughly $\epsilon_M/a_B \approx 30$ pN or torques on the order of $\epsilon_M/\psi_B \approx \pm 17$ pN nm, B-DNA will undergo transformations to other dsDNA structures (recall that near room temperature, $k_B T \approx 4.1$ pN nm). We note the appreciable sequence dependence of ϵ_M, which varies from 1 for AT-rich sequences to 4 $k_B T$ for GC-rich sequences [12].

Single-molecule experiments carried out over the past 20 years have discovered a menagerie of dsDNA structural states, connected by first-order-like pseudo phase transitions occurring at approximately these force and torque scales. One of the first of these alternative structures to be characterized, "overstretched," or S-DNA, was found to be about 1.7 times longer than B-DNA and was observed to form via a constant-force "plateau" at about 65 pN for molecules under no torsional constraint (zero torque) [13,14]. The sharp force plateau suggested description in terms of a first-order-like phase transition between a low-free energy B state and a longer but higher-free energy S state, in analogy with the constant pressure between coexisting liquid and gas phases seen as volume is changed. A number of two-state models have been used to interpret the B-S transition in terms of a model of S-DNA as an at least partially base-paired state [13,15–18]. An alternative hypothesis was that S-DNA was essentially force melted [19–21]; an important idea needed to understand the

experimental data was consideration of competition between
S-DNA and "unpeeling" of one strand from the other, which
occurs in experiments with "nicked" molecules (double helices
with one or more breaks in the sugar-phosphate backbones)
[18,22,23]. In the past few years, a series of experiments aimed
at discerning base-unpaired from base-paired DNA structures
have gradually strengthened the hypothesis that overstretched
DNA is at least partially base paired [22–26].

Other researchers succeeded in "unzipping" the two strands
of B-DNA by pulling them away from one another [27].
Unzipping was observed to occur via a force plateau of
≈12 pN, and with fine structure reflecting the known variation
of ϵ_M with sequence. Combining the known elastic response of
the unzipped single-stranded DNAs (ssDNA) and the known
sequence variation of ϵ_M led to models able to quantitatively
describe DNA unzipping [28,29].

The variety of structural transformations possible for
dsDNA was greatly increased by experiments with torsionally
constrained molecules, which measured dsDNA extension
versus force for experimentally controlled linking number
[30]. Further work has established methods to measure
DNA torque, leading to experiments where extension versus
force and linking number versus torque (i.e., both pairs of
extensive and intensive variables in a DNA stretching-twisting
experiments) can be simultaneously measured [31–37].

A relaxed B-DNA of contour length L has a double helix
linking number of approximately one right-handed turn per
10.5 bp or $\mathrm{Lk}_0 = +(L/a_B)/n_B = +(L/a_B)\psi_B/(2\pi)$, where
L is the relaxed B-form contour length. Changes in DNA
linking number are usually referenced relative to Lk_0 through
the extensive $\Delta \mathrm{Lk} \equiv \mathrm{Lk} - \mathrm{Lk}_0$ or through the density of
linking number change, $\sigma \equiv \Delta \mathrm{Lk}/\mathrm{Lk}_0$. Note that completely
separated single strands have $\mathrm{Lk} = 0$ or $\sigma = -1$. Molecular
structure simulations have shown that stereochemistry of the
DNA strands limits linking number to the range $-6 < \sigma < +4$
[38].

Experiments on underwound molecules revealed that DNA
could transform into an alternative state with a linking number
of roughly $\sigma \approx -2$, corresponding to a left-handed double
helix with a well-defined contour length somewhat longer than
that of B-DNA, at a torque of ≈ -10 pN nm [16,31,39]. At
low forces (<3 pN) this state has zero length, while, at higher
forces, it appears to behave as a rather soft but still semiflexible
polymer [36]. This state has come to be called "L-DNA," the
L denoting "left-handed" [31,36]. L-DNA has a net helicity
similar to the "Z" form taken by GC-rich DNA sequences
under some chemical conditions and has been argued to be at
least partially made up of Z-DNA [37]. L and S are structurally
distinct; S is less strongly underwound ($\sigma \approx -0.7$ [16,39]) but
still right handed.

For overwinding, it was found that for torques $\approx +40$ pN
nm, a highly overwound ($\sigma \approx +3$) state about 1.7 times
longer than the B form occurred [38]. Because of the extreme
overwinding it was hypothesized that this state had its sugar-
phosphate backbones in the *middle* of the double helix, with
the unpaired bases exposed. This state was named "P-DNA,"
after a model of Pauling for the double helix with a somewhat
similar structure.

Given the appreciable experimental data describing these
various alternative DNA structures, plus the rather successful

application of mesoscopic descriptions of supercoiling of
semiflexible polymers with twist rigidity to the description of
supercoiling of B-DNA, we set out to construct a free-energy-
based model of DNA structural transitions. Our approach
considers each of the B, L, P, and S states as semiflexible
polymers, allowing their supercoiled forms to appear naturally
using suitable generalization of the mesoscopic model of
plectonemic supercoiling previously applied only to B-DNA
[3–9]. The result is a theory with unified low-force supercoiled
states and high-force extended states in a way consistent
with current experimental data. The model predicts lines of
first-order-like transitions in the force-torque plane, connected
at triple points.

A surprise arising from the model is the appearance of two
distinct types of plectonemic supercoiling: Supercoils can be
"inflated" by thermal fluctuation and electrostatic repulsion
or they can be "collapsed," with juxtaposed double helices
driven to close contact [7,8]. We find that in physiological
solution conditions B- and L-DNA supercoil to form inflated
plectonemes but that supercoiled P-DNA is always collapsed.

Finally, experimental data suggest that fully denatured
(force-melted parallel ssDNAs) DNA, plus a strongly under-
wound "Q" state of DNA, analogous to left-handed P-DNA
($\sigma \approx -5$), and its collapsed supercoiled form are needed to
complete the theory [36,38]. Including these states provides a
rather complete description of DNA states over forces up to
1000 pN and over a torque range from -60 to $+60$ pN nm.

II. MODEL

Our approach is similar to prior theories of supercoiling
of B-DNA [3–9,40]. We compute free energies per base
pair for candidate states, in the ensemble of fixed force and
torque, $\Phi_i(f,\tau)$, where i is the state label. We consider
the long-molecule limit and adopt the simplification of
considering single plectonemic DNA domains (for B-DNA,
at physiological univalent salt concentrations ≈150 mM this
is a good approximation [9]). The zero of free energy is taken
to be that of relaxed B-DNA; in particular, linking number will
be considered relative to that of relaxed B-DNA.

For any of the states, the average linking number may be
expressed as a rotation angle per base pair ψ relative to the
angle of rotation per base pair ψ_B of the relaxed B-DNA state
(i.e., $\Delta\psi = \psi - \psi_B$). The average $\Delta\psi$ and the end-to-end
extension x per base pair follow from the free energy via [41]

$$x = -\frac{\partial \Phi_i}{\partial f}, \quad \Delta\psi = -\frac{\partial \Phi_i}{\partial \tau}. \tag{1}$$

The angle change $\Delta\psi$ is convenient since it is given by the
torque derivative of Φ_i. It is also straightforward to relate
to DNA structure, being just the rotation angle per base
pair in excess of ψ_B for a straight molecule. The linking
number density σ is proportional to $\Delta\psi$, the proportionality
factor being the relaxed B-form rotation angle per base pair,
$\sigma = \Delta\psi/\psi_B$.

The free energy Φ_i is connected to the more familiar
free energy per base pair at fixed force and linking number,
$\mathcal{F}(f,\Delta\psi)$, by Legendre transformation

$$\Phi_i(f,\tau) = \mathcal{F}_i(f,\Delta\psi) - \tau\,\Delta\psi. \tag{2}$$

In the "intensive" f-τ ensemble, the stable state at each f-τ point is that with the lowest Φ_i. Structural transitions occur when the free energies of states cross. In the force-torque plane, one is destined to obtain a series of phase boundary curves between pairs of states. Along these curves, there is two-state coexistence; the two coexisting states will generally have different extensions and linking numbers. Phase coexistence curves will generally meet at triple points where three phases coexist. Higher-order coexistence points are not generic in the f-τ plane but could be found in a higher-dimensional phase diagram (e.g., one can expect four-phase coexistence points in the three-dimensional f-τ-temperature spaces).

Regarding the generic "first-order" nature of the transitions that will be considered, in actual experiments one has a finite-length, one-dimensional molecule, and there can be no "real" phase transitions (i.e., free energy singularities). On top of this, sequence inhomogeneity of real DNAs will further smooth the transitions. Nonetheless, experiments do observe quite sharp DNA structural transitions and clear regimes of apparent phase coexistence as linking number is varied [13,16,31,34,36,39]. This is likely due to the relatively large and rapid changes in free energy that occur as one passes from one state to the other and due to the energies of interfaces between different states also being several $k_B T$ in size. We compute and describe sharp transitions while keeping in mind that finite-length, finite-temperature and sequence-disorder effects can be expected to smear transitions observed in experiments.

A. Semiflexible polymer under force and torque

We begin with the model for a single semiflexible polymer chain in the f-τ ensemble, which will be used to describe the B, L, S, P, and Q states. In the force-linking number ensemble the molecule is described by a stretching free energy g which depends on applied force plus a twisting free energy contribution [42,43]. The free energy per base pair is

$$\mathcal{F}_i = \left[-g_i + \frac{1}{2} k_B T C_{f,i} \left(\frac{\Delta\psi - (\psi_i - \psi_B)}{a_i} \right)^2 \right] a_i + \epsilon_i,$$
(3)

where a_i is the contour length per base pair and where ϵ_i is the "creation" free energy per base pair of state i (ϵ_B will be taken to be zero). This can be also expressed in terms of $\sigma = \Delta\psi/\psi_B$ and the preferred linking number density of state i, $\sigma_i = \psi_i/\psi_B - 1$. The i subscripts in (3) indicate use of parameters for a specific DNA state (i = B, L, S, P, or Q).

Here $g(f)$ is the free energy per contour length of the semiflexible polymer at fixed force; this could include contour length stretching or other effects that might depend on state i. For our purposes the high-force limit of the inextensible semiflexible polymer $g(f) = f(1 - \sqrt{k_B T/(Af)})$, where A is the bending persistence length, will suffice as we will not consider forces below the limit of validity of $Af < k_B T$.

The fluctuation-renormalized twist persistence length C_f is the lowest-order contribution from the $1/\sqrt{f}$ expansion of Moroz and Nelson [42], $C_f = C[1 - (C/4A)\sqrt{k_B T/(Af)}]$, where C is the bare twist persistence length. Given the classical buckling instability occurring at $4k_B T A f = \tau^2$ [44], which puts a hard limit on the region of validity for the Gaussian

fluctuation theory from which C_f is derived [42], we will not consider the extended state to exist for $4k_B T A f < \tau^2$.

The torque is the rate of work done per base pair as linking angle per base pair is changed,

$$\tau = \frac{\partial\mathcal{F}_i}{\partial\Delta\psi} = \frac{k_B T C_{f,i}}{a_i} \left[\Delta\psi - (\psi_i - \psi_B) \right],$$
(4)

which allows the free energy (3) to be transformed to the force-torque ensemble using the Legendre transformation (2),

$$\Phi_i(f,\tau) = -\left[g_i(f) + \frac{\tau^2}{2k_B T C_{f,i}} \right] a_i - (\psi_i - \psi_B)\tau + \epsilon_i.$$
(5)

B. Plectonemic supercoiling of semiflexible polymer

The free energy per base pair for a plectonemic supercoil polymer does not depend on force, since its end-to-end extension is zero [43]. Following prior work [3–9], we model the plectoneme as a regular helix of radius R and opening angle α; R and α will be treated as variational parameters to optimize the free energy.

In the fixed force-linking number ensemble, we write

$$\mathcal{F}_{\text{plect},i} = \left[\frac{1}{2} k_B T A_i \frac{\sin^4\alpha}{R^2} + \frac{1}{2} k_B T C_i \left(\frac{\Delta\psi - (\psi_i - \psi_B)}{a_i} \right. \right.$$
$$\left. \left. + \frac{\sin 2\alpha}{2R} \right)^2 + U_i(R) \right] a_i + \epsilon_i.$$
(6)

The term proportional to A_i is the bending energy per base pair due to the helical conformation. The term proportional to C_i is the twisting free energy per length, which is obtained from the usual twist energy for a supercoil involving a length L of polymer, $(k_B T C_i/2)(2\pi \text{Tw}/L - \psi_i/a_i)^2$, including the preferred rotation angle per base pair ψ_i. The twist energy in (6) is obtained from this using the definition of the linking angle per base pair, $\Delta\psi = (2\pi \Delta\text{Lk})(a_i/L)$, White's theorem $\text{Lk} = \text{Tw} + \text{Wr}$, and the writhe per length for a plectonemic supercoil $\text{Wr}/L = -(\sin 2\alpha)/(4\pi R)$. The sign of the writhe depends on plectoneme chirality, controlled by the sign of α; for right-handed coiling $\alpha > 0$ and $\text{Wr} < 0$; for left-handed coiling $\alpha < 0$ and $\text{Wr} > 0$.

The last term U_i takes into account the free energy associated with electrostatic interaction between the adjacent polymers in the supercoil and the entropy cost of confinement of the polymers in a supercoil of radius R; both of these contributions are repulsive. The detailed form of U_i is discussed in Sec. II B 1.

The torque is the rate of change of free energy with linking angle,

$$\tau = \frac{\partial\mathcal{F}_{\text{plect},i}}{\partial\Delta\psi} = \frac{k_B T C_i}{a_i} \left[\Delta\psi - (\psi_i - \psi_B) + \frac{a_i \sin 2\alpha}{2R} \right]$$
(7)

and the fixed-torque free energy is computed by Legendre transformation (2)

$$\Phi_{\text{plect},i} = \left\{ \frac{1}{2} k_B T A_i \frac{\sin^4\alpha}{R^2} - \frac{\tau^2}{2k_B T C_i} + \tau \frac{\sin 2\alpha}{2R} + U_i(R) \right\}$$
$$\times a_i - (\psi_i - \psi_B)\tau + \epsilon_i.$$
(8)

This free energy is used to introduce plectonemic supercoiling of the semiflexible polymer states in the theory (B, L, P, S, and Q) without any additional parameters.

1. Electrostatic interaction and confinement entropy in the plectoneme

The dsDNA-dsDNA interaction free energy per length is made up of electrostatic and entropic contributions [3,8] as follows:

$$U_i(R) = U_{\text{el},i}(R) + U_{\text{ent},i}(R). \tag{9}$$

The electrostatic contribution is taken to be that of Stigter [45] for the interaction energy per length for two parallel chains at distance $2R$ apart,

$$U_{\text{el},i}(R) = k_B T \nu_i^2 L_B K_0(2\kappa_D R), \tag{10}$$

where $K_i(x)$ is the ith modified Bessel function of the second kind and where $L_B = e^2/(\epsilon k_B T) = 0.703592$ nm is the Bjerrum length for water at room temperature (296.5 K or 23.35 °C, the temperature used for all computations in this paper) and where $1/\kappa_D$ is the Debye length. For univalent (1:1) salt at concentration M in water at 296.5 K, $1/\kappa_D = 0.306439 M^{-1/2}$ nm.

We follow the procedure of Stigter [45] for determining the effective linear charge density $e \nu_i$; see also Appendix B. This procedure requires the linear bare charge density and the charge radius ρ_i (the location of the charges) as inputs. For B-DNA we use a linear bare charge density of 0.17 e/nm (two electron charges per base pair of length $a_B = 0.34$ nm) and a charge radius ρ_B equal to the molecule hard-core radius $R_{0,B} = 1.0$ nm. For other than B-DNA forms, we rescale the linear bare charge density by a factor of a_B/a_i, and we rescale the molecule radius to $R_{0,i} = \sqrt{a_B/a_i} R_0$ (conserving volume) to compute the effective charge. For all DNA forms except P and Q the charge radius ρ_i is taken to be equal to the molecule radius $R_{0,i}$. For P- and Q-DNA forms we set $\rho_P = \rho_Q = 0.15$ nm due to the inward positioning of the sugar-phosphate backbone [38]. The final electrostatic parameters used are listed in Table I for 150 mM salt (roughly physiological, the case focused on here) as well as a number of other commonly studied salt concentrations.

The entropic interaction is taken to be that for a semiflexible polymer confined in a tube of the superhelix radius R

TABLE I. B-DNA persistence length and effective charges for various DNA forms for 1:1 salt concentrations between 10 and 500 mM, pH 7.5, $T = 296.5$ K. The ν_i are computed as described in the text using $a_L = 1.35 a_B$ and $a_P = a_Q = a_S = 1.7 a_B$. Note $\nu_P = \nu_Q$, due to the same length per base and charge radius ($\rho_P = \rho_Q = 0.15$ nm) used for the P and Q states.

1:1 salt (mM)	A_B (nm)	ν_B (nm^{-1})	ν_L (nm^{-1})	ν_P, ν_Q (nm^{-1})	ν_S (nm^{-1})
10	53	2.4102	2.0872	1.3272	1.8802
50	48	4.0357	3.2420	1.5102	2.7218
150	45	7.2148	5.2268	1.7424	4.1166
500	43	20.4262	12.4326	2.1573	8.6702

[3,4,46,47],

$$U_{\text{ent},i}(R) = \frac{k_B T}{2(A_i R^2)^{1/3}}. \tag{11}$$

A few comments are in order regarding approximations made in the model of plectonemic supercoiling used here. First, the form of the electrostatic interaction is that for two *parallel* charged rods and is therefore dependent on only the plectoneme radius. This approximation is reasonable since the opening angles α of stable plectonemic supercoils tend to be quite small to minimize bending energy [4–9] and thus not far from parallel DNAs in geometry.

Second, *branching* of the plectonemic domains is not considered (approximately one branch point per kilobase [4,48,49] is expected); while this will certainly affect the geometry of the plectonemic state, the free energy associated with this will be less than $10^{-2} k_B T/$nm and not a large contribution. Furthermore, the relatively short dsDNAs studied using single-DNA methods (typically smaller than 10 kb) will not have highly branched plectonemic domains. Similarly, plectonemic axis bending entropy is not included, but this will contribute a free energy density on the order of a $k_B T$ per 100 nm (the persistence length of a plectonemic structure will be roughly that of *two* parallel DNAs), which is, again, a relatively small contribution to the free energies considered in this paper.

Finally, we note that the confinement free energy is not dependent on the helical geometry of the supercoil in the present treatment; again, this is permissible given the small-α solutions typical for models of plectonemic supercoiling. However, all of these approximations are important to keep in mind for future development of the model.

2. Optimization of plectoneme geometry

We seek R and α values that minimize the plectonemic phase free energy (8); in this subsection we drop the DNA state index i from A_i, C_i, ν_i, a_i, and U_i as we are considering just one of the states. We focus on terms with R and α dependence, writing $\Phi_{\text{plect}} = \phi(\alpha, R) + \text{const.}$ with

$$\phi(\alpha, R) = \frac{1}{2} k_B T A \frac{\sin^4 \alpha}{R^2} + \tau \frac{\sin 2\alpha}{2R} + U(R). \tag{12}$$

We note that ϕ depends on torque τ but has no force dependence due to the zero extension of the plectoneme state. Minimizing ϕ with respect to α and R requires solution of
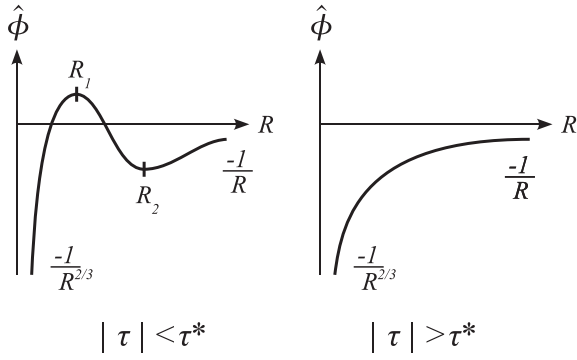
$$\frac{\partial \phi}{\partial \alpha} = \frac{2 k_B T A}{R^2} \sin^3 \alpha \cos \alpha + \tau \frac{\cos 2\alpha}{R} = 0, \tag{13a}$$

$$\frac{\partial \phi}{\partial R} = -k_B T A \frac{\sin^4 \alpha}{R^3} - \tau \frac{\sin 2\alpha}{2R^2} + U'(R) = 0. \tag{13b}$$

Equation (13a) yields

$$\frac{\sin^3 \alpha \cos \alpha}{\cos 2\alpha} = -\frac{\tau R}{2 k_B T A}, \tag{14}$$

indicating that α and τ have opposite signs and that $|\alpha| < \pi/4$ and increases with $|\tau| R$. At fixed τ, we solve (14) for $0 < R < \infty$ to obtain $\alpha = \alpha(R)$, leading to $\hat{\phi}(R) = \phi(\alpha(R), R)$. Using

FIG. 1. $\hat{\phi}(R)$ for small (left) and large (right) torques τ.

(14) we have

$$\hat{\phi}(R) = (\tau/4R)\,(1 + 2\cos^2\alpha)\tan\alpha + U(R). \qquad (15)$$

In the remainder of this subsection we focus on the electrostatic portion (10) of $U(R)$ as this allows relatively straightforward analysis of behavior of the minima. Effects of the entropic term (11) can be quantitatively important but do not change the qualitative properties of the analysis.

3. Behavior of R(τ): Mechanism of plectoneme "collapse" for large torques

For the sake of clarity we deal here with the case $\tau \geqslant 0$ (symmetrical results are found in the case $\tau \leqslant 0$). For small R, Eq. (14) yields $\alpha \approx -(\tau/[2k_BT])^{1/3}(R/A)^{1/3}$ and, hence, $\hat{\phi}(R) \approx -2^{-1/3}(k_BT/A)(\tau/k_BT)^{4/3}(A/R)^{2/3}$ [note the accidental coincidence of the R dependence with the $+R^{-2/3}$ behavior of the entropic portion of $U(R)$]. For large R, $\alpha \to -\pi/4$ and $\hat{\phi}(R) \approx -\tau/(4R)$; $\hat{\phi} \to 0^-$ as $R \to \infty$. Hence both small- and large-R limits are dominated by elastic terms [i.e., the first term in the right-hand side of (15)]. However, for intermediate R and provided τ is not too large, $|\tau| < \tau^\star$, the potential $U(R)$ comes into play and introduces one local maximum (at $R = R_1$) and one local minimum

(at $R = R_2 > R_1$) in the energy $\hat{\phi}(R)$ (Fig. 1, left panel). The state $R_2(\tau)$ is the usual plectoneme state, which we describe as "inflated" by the repulsive potential $U(R)$.

A key question is whether the loci R_1 and R_2, the two branches of $R(\tau)$, meet for finite torque τ and whether for large torques there is no longer a solution of (13). This scenario is shown in the right panel of Fig. 1. Solving (13) numerically, we compute R_1 and R_2 as functions of τ and indeed find that for sufficiently large τ (13) has no solution; see Fig. 2 (plotted for B-DNA at 10, 50, and 150 mM univalent salt; $R_{0,B} = 1.0$ nm, $a_B = 0.34$ nm, A_B and ν as in Table I). In both cases, as τ is increased, R_1 increases while R_2 decreases; R_1 meets R_2 at a "fold point" $\tau = \tau^\star$ and $R_1(\tau^\star) = R_2(\tau^\star) = R^\star$, where the local maximum R_1 and the local minimum R_2 "annihilate" one another.

This behavior is generic (persistent for different choices of parameters): beyond a finite torque τ^*, there is no more "inflated," locally stable plectonemic state [7,8]. Examination of (15) shows that the physical mechanism is the power-law dependence of the writhe on R; as τ is increased, the $1/R$ term dominates, eventually eliminating the possibility of a solution to (13). For $\tau > \tau^*$ the lowest free-energy state suddenly becomes a boundary minimum determined by the smallest sterically allowed value of R. We describe such a state as a "collapsed" plectoneme.

Figure 2(a) shows that the scale for the fold-point torque τ^* depends strongly on salt concentration. For 150 mM salt, the fold point and elimination of a barrier to collapse occurs for very large torques $\approx$140 pN nm. For 10 mM salt, the fold-point torque is reduced to $\approx$50 pN nm.

4. Asymptotic formulas for R₁ and R₂

Approximations for $R_1(\tau)$ and $R_2(\tau)$ can be obtained from the large-R and small-R asymptotic solutions of (13a). We use (13a) to transform (13b) to

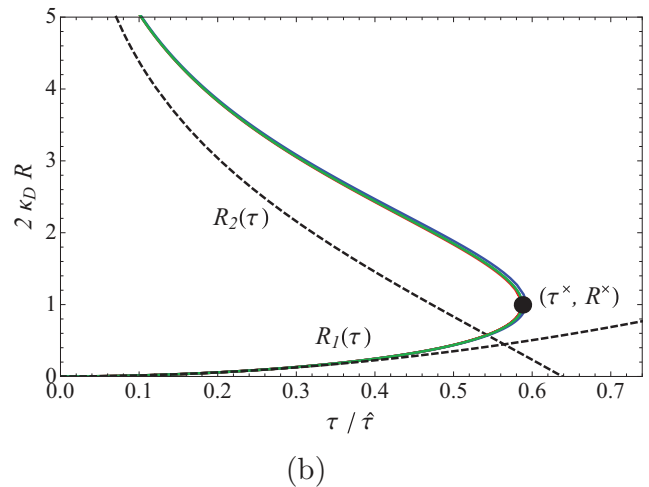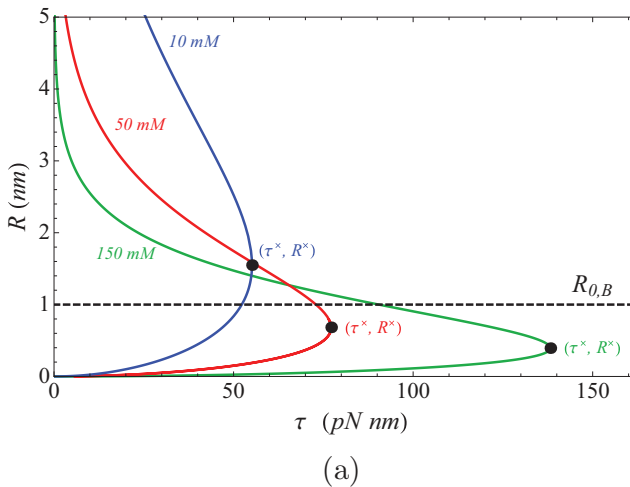$$U'(R) - \frac{\tau}{2R^2}\tan\alpha = 0. \qquad (16)$$

(a)

(b)

FIG. 2. (Color online) Plectonemic radius R as function of applied torque τ. (a) $R(\tau)$ for B-DNA in 150, 50, and 10 mM univalent salt. Note that the fold-point torque τ^* (the peak values of torque) becomes progressively larger with increasing salt concentration. (b) $R(\tau)$ in dimensionless scaling variables. Dotted curves are the small- and large-R asymptotic solutions (17) and (19), and the solid curves correspond to nonlinear solutions (13) for B-DNA in 150, 50, and 10 mM univalent salt. Note the strong collapse of these nonlinear solutions by this scaling.

From (14) we obtain the approximation $\tan\alpha \simeq \alpha \simeq -(\tau R/[2k_B T A])^{1/3}$, which we use for both $R_1(\tau)$ and $R_2(\tau)$.[1] This is inserted into (16) which now becomes an equation for R only. From (10) we have $U'(R) = -2\kappa_D k_B T \nu^2 L_B K_1(2\kappa_D R)$; asymptotic closed-form expressions may be obtained using $K_1(z) \simeq \sqrt{\pi/2}\, e^{-z}/\sqrt{z}$ for large z and $K_1(z) \simeq 1/z$ for small z.

In the small-R limit (16) is approximated by

$$2\kappa_D R_1(\tau) \simeq \left(\frac{\pi}{2}\right)^{3/4} \left(\frac{\tau}{\hat\tau}\right)^2, \tag{17}$$

where $\hat\tau = 2^{1/8} \pi^{3/8} k_B T\, A^{1/4} L_B^{3/4} \nu^{3/2} \kappa_D^{-1/2}$ determines the scale for torque.

In the large-R limit (16) reduces to $\tau^{4/3} = \hat\tau^{4/3} z^{7/6} e^{-z}$, where $z = 2\kappa_D R$. Applying a log to both sides yields

$$z - \frac{7}{6}\log(z) = \frac{4}{3}\log\left(\frac{\hat\tau}{\tau}\right). \tag{18}$$

As this is not solvable in closed form, we neglect $\log(z)$ in favor of z to obtain a first approximation $z_0 = \frac{4}{3}\log(\frac{\hat\tau}{\tau})$ which can then be corrected to the next order in $\log(z)$ as follows:

$$2\kappa_D R_2(\tau) \simeq \frac{4}{3}\log\left(\frac{\hat\tau}{\tau}\right) + \frac{7}{6}\log\left[\frac{4}{3}\log\left(\frac{\hat\tau}{\tau}\right)\right]. \tag{19}$$

The approximations $R_1(\tau)$ and $R_2(\tau)$ are plotted in Fig. 2(b) together with full nonlinear solutions of (13) for B-DNA in 10, 50, and 150 mM salt. As seen in formula (17) and (19), $\kappa_D R_1$ and $\kappa_D R_2$ depend on only one dimensionless torque scaling variable $\tau/\hat\tau$, but the full nonlinear solution of (13) does not have this simple scaling form and depends on multiple combinations of $\tau/(k_B T)$ and dimensionless combinations of the lengths κ_D^{-1}, ν^{-1}, L_B, and A. Nevertheless, Fig. 2(b) clearly shows that this solution is close to being just a function of the scaled variable $\tau/\hat\tau$. Consequently a numerical approximation to the fold point $(R^\star, \tau^\star)$ is directly read from Fig. 2(b) to be $\tau^\star \simeq 0.6\,\hat\tau$ and $2\kappa_D R^\star \simeq 1$.

5. Hard-core radius determines whether plectoneme collapse is discontinuous or continuous

We have seen in the previous subsection how competition between elastic and interaction contributions to the plectoneme free energy is controlled by torque τ. For small $|\tau|$ the plectoneme is "inflated" by the potential $U(R)$ to have radius $R_2(\tau)$ (Fig. 1). As $|\tau|$ exceeds the threshold $\tau^\star \propto k_B T\, A^{1/4} L_B^{3/4} \nu^{3/2} \kappa_D^{-1/2}$, the elastic terms dominate and the system falls into a "potential hole," with free energy minimized by $R \to 0$ (see Fig. 1). The unphysical $R \to 0$ behavior is cut off by the addition of the steric lower limit $R \geqslant R_{0,i}$, where $R_{0,i}$ is the hard-core contact radius for phase i. Cases with a boundary minimum $R = R_{0,i}$ are "collapsed" configurations. We emphasize that this collapse occurs in the absence of any explicitly attractive interactions between double helicies: Instead, the elastic forces overwhelm the electrostatic and other
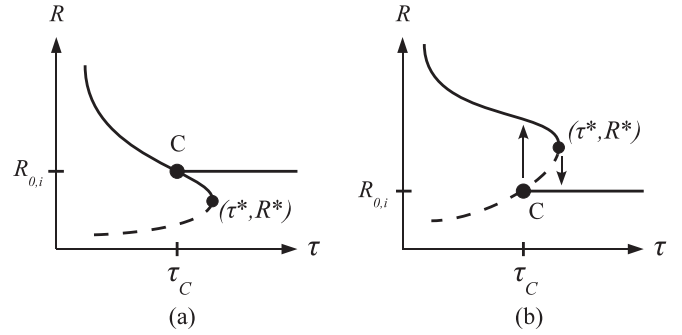
---

[1]An explicit formula for α as a function of R can be obtained, $\alpha = \arctan[(-u/(1+u))^{1/4}]$ with $u = R^3 U'(R)/(k_B T A)$, but this does not improve the present approximations.

FIG. 3. Plectonemic collapse scenarios. Superhelix radius R decreases with increasing τ. Depending of the position of point C $(\tau_C, R_{0,i})$ relative to the fold $(\tau^\star, R^\star)$, the transition from an inflated state to a collapsed state can be either (a) continuous or (b) abrupt.

repulsions and drive the double helices in the plectoneme to be essentially in molecular contact. We also note that prior theories of plectonemic supercoiling with repulsive DNA-DNA potentials have not been forced to confront this situation due to the large torques associated with the collapse of plectonemic B-DNA [3–5]. We nevertheless remark that collapsed solutions were mentioned in Refs. [7,8].

Figure 3 illustrates that there are in fact two scenarios for plectoneme collapse driven by gradually increased torque, depending on whether the collapsed state (point C), defined as $R(\tau_C) = R_{0,i}$, lies [Fig. 3(a)] in the upper (stable) or [Fig. 3(b)] lower (unstable) part of the $R(\tau)$ curve. As τ is increased from small values, the superhelix radius R decreases. In Fig. 3(a), the collapse transition is second-order-like, with R decreasing smoothly to $R_{0,i}$. In Fig. 3(b), there is a discontinuous, first-order-like transition where the superhelix radius jumps $R^\star \to R_{0,i}$ at $\tau^\star$. If τ is subsequently decreased in this second case, hysteresis could be observed with a jump $R_{0,i} \to R_2(\tau_C)$ at $\tau_C < \tau^\star$ [Fig. 3(b)].

We have not here included the entropic confinement potential contribution, $U_{\rm ent} \approx (k_B T/A)(A/R)^{2/3}$. Despite $U_{\rm ent}$ having the same R dependence and opposite sign of the $R \to 0$ limit of $\hat\phi$, the extra factor of $[\tau/(k_B T)]^{4/3}$ in the latter relative to the former generally will make the elastic terms in $\hat\phi$ dominate over the confinement entropy term, since in most cases we will be considering supercoiled states driven by torques $\tau \gg k_B T$. In the opposite limit of large R, the same consideration applies (the $-1/R$ term in $\hat\phi$ is amplified by a factor of τ) and will not qualitatively alter $\hat\phi$ in most situations we will consider (it also should be noted that we are not concerned with the case where R is comparable to or larger than A, where one enters the flexible-polymer regime). The general picture we have outlined has its numerical details altered when $U_{\rm ent}$ is included, but the qualitative behavior of Fig. 2 and the scenarios of Fig. 3 continue to apply.

In the following it will be shown that for reasonable choices of elastic parameters and including $U_{\rm ent}$, collapsed configurations of plectonemically supercoiled B-DNA are *never* stable for physiological (150 mM) salt. This can be anticipated from Fig. 2(a) since the 150 mM curve has its fold point at such a large torque (140 pN nm) that structural transitions to other states will always preempt plectoneme collapse. Similarly, we find L-DNA to be generally inflated. In

contrast, we find the stable supercoiled P- and Q-DNA states to *always* be collapsed, consistent with the large torques and stretching-weakened electrostatic interactions associated with their creation.

C. Unwound parallel single strands

In addition to double-helix B, L, P, Q, and S extended and plectonemic states, we consider the possibility of two entirely separated single-stranded DNAs (ssDNAs), with linking number $\sigma = -1$. The maximum contour length of ssDNA is about double that of B-DNA, but ssDNA has a short persistence length, making it extend to such extensions only for forces beyond ≈ 10 pN.

For this state, we use an empirical formula [18] based on experimental data for the extension per base of one ssDNA:

$$x_{ss}(f) = a_1 \ln(f/f_1) - a_2 e^{-f/f_2}. \tag{20}$$

This gives the logarithm-shaped response which is characteristic of ssDNA and quite distinct from semiflexible polymer elasticity [14,50,51]. Depending on a_2, the extension cuts off to zero at a force threshold f_0, determined by $x(f = f_0) = 0$; this is a crude model for formation of secondary structure which tends to make ssDNA stick to itself and contract at low forces.

Parameters that lead to a force curve that fits data for 150 mM salt well are as follows: $a_1 = 0.07$ nm, $f_1 = 0.015$ pN, $a_2 = 0.8$ nm, and $f_2 = 2.5$ pN. For lower-salt conditions, lowering a_2 provides a reasonable description; for example, data for 2.5 mM NaCl are fit fairly well by $a_2 = 0.1$ nm [52]. In the extreme low-salt limit, a nearly purely logarithmic force-extension curve is observed which has been justified theoretically [50,52–54]; such an elastic response is obtained by setting $a_2 = 0$.

To obtain the fixed-force free energy per base for a ssDNA, one integrates the following extension:

$$\begin{aligned} g_{ss}(f) = \int_{f_0}^{f} df\, x(f) &= a_1(f \ln f - f_0 \ln f_0) \\ &- a_1(1 + \ln f_1)(f - f_0) \\ &+ a_2 f_2 (e^{-f/f_2} - e^{-f_0/f_2}). \end{aligned} \tag{21}$$

To obtain the free energy for two parallel ssDNAs (referred to in what follows as the "2ss" state) we split the force between the two strands and add the free energy per base pair associated with separating dsDNA into two ssDNAs at zero force, ϵ_M:

$$\Phi_{2ss}(f) = 2g_{ss}(f/2) + \epsilon_M + \psi_B \tau. \tag{22}$$

The strand separation free energy per base pair ϵ_M is known from measurements of DNA melting and averages to ≈ 2.5 $k_B T$. The linear-τ term gives the average linking angle for the parallel ssDNAs of $\Delta \psi = -\psi_B$ or $\sigma = -1$, i.e., fully unwound DNAs. In this paper we take $\epsilon_M = 2.7 k_B T + 0.2 k_B T \ln(M/150\text{mM})$, where M is the solution concentration of univalent ions [18]. The logarithmic dependence of ϵ_M on M is commonly found in models for strand-separation free energy and fits well to experimental data [12].

We add no torque dependence to this parallel-ssDNA free energy for a few reasons. First, this gives us a model where the strands are always unwound ($\partial \Phi_{2ss}/\partial \tau = \psi_{ss} - \psi_B$) for

which the elastic model (22) applies. If we were to have quadratic torque dependence, we would also need to take into account the contraction of the two ssDNAs and the modification of their elasticity as they were wound around one another, making (22) inapplicable. Furthermore, tightly wound fully unpaired ssDNAs are already accounted for in our model, in the form of P-DNA and its reversed Q-DNA form. Finally, braided flexible polymers actually are expected to behave as if they have a very large torsional modulus, due to the large amount of entropy that they need to give up to be braided together [55,56], leading back to (22) (note that this high braiding torsional modulus will tend to drive "phase separation" of braiding, generating essentially the 2ss state in coexistence with tightly wound states already in the model [55,56]). The model (22) is a simple way to obtain an estimate of the free energy for fully strand-separated DNA.

III. RESULTS

A. Semiflexible polymer parameters for DNA states

For each semiflexible chain state (B-, L-, P-, Q-, and S-DNA), we need to choose the contour length per base pair a_i, the preferred helical rotation angle per base pair ψ_i, the bend and twist persistence lengths A_i and C_i, and the state creation free energy per base pair ϵ_i. As previously discussed, the hard-core radii $R_{0,i}$ are determined by the a_i. The effective charge density $e\, v_i$ is determined by the a_i and the charge radii ρ_i. For states B, L, and S the charge radii are taken to be equal to the hard-core radii $\rho_i = R_{0,i}$, whereas for states P and Q $\rho_i \neq R_{0,i}$, a result of the inward orientation of the phosphate backbone. We take $\rho_P = \rho_Q = 0.15$ nm. Most of the structural parameters are fixed by experimental measurement; the free energy offsets ϵ_i can be estimated from experimental information. Our objective here is to estimate suitable parameters for solution with 150 mM univalent salt (typically NaCl, KCl, or KGlu).

1. B-DNA

For B-DNA, $\epsilon_B = 0$, $\psi_B = 2\pi/10.5 = 0.598398$, $a_B = 0.34$ nm, and $C_B = 95$ nm. The bending persistence length varies slightly with univalent ion concentration (see Table I); for 150 mM salt, we take $A_B = 45$ nm [32].

At 150 mM salt, $f = 3$ pN, and $\tau = 5$ pN nm we have $\Phi_B = -0.209\, k_B T$ and $\Phi_{\text{plect},B} = -0.011\, k_B T$.

2. L-DNA

Sheinin *et al.* [36] determined L-DNA to be about 1.4 times longer than B-DNA in length, to have persistence lengths $A_L = 4 \pm 2$ nm and $C_L = 15 \pm 5$ nm, and to be a left-handed helix with a 15-bp repeat. The length and helicity values agree well with older measurements [16,31,39] as well as with recent experiments [37].

Here we take $a_L = 1.35 a_B = 0.4590$ nm, $A_L = 7$ nm, $C_L = 19$ nm, and $\psi_L = -2\pi/16 = -0.392699$. We will show that these parameters reproduce the experimentally observed force-extension behavior [36] for "pure" L-DNA along the B-L coexistence line.

Sheinin *et al.* [36] found that there was little variation of the critical torque ≈ 10 pN nm for creation of L-DNA at forces

below $\approx$5 pN, in accord with theoretical prediction [16] and other experimental measurements [31,35,37]. It is reasonable to estimate that the creation energy for L-DNA is roughly the work done by the applied torque in that force regime. We estimate that $\epsilon_L \approx (10$ pN nm$)|\psi_L - \psi_B| \approx 2.5$ $k_B T$. This estimate is very close to the free energy of melting (ϵ_M), which is encouraging since L-DNA is thought to be at least in part torque-melted [36,37]. For this paper we take $\epsilon_L = \epsilon_M - 0.2$.

At 150 mM salt, $f = 3$ pN, and $\tau = 5$ pN nm we have $\Phi_L = 3.497\,k_B T$ and $\Phi_{\mathrm{plect},L} = 3.682\,k_B T$.

3. P-DNA

Allemand *et al.* [38] found P-DNA to have $a_P = 1.7a_B$ and to have a helix repeat of about 3 bp; they also estimated the persistence length for 10 mM salt to be $A_P = 19$ nm. While data are not published for the twist persistence length of P-DNA, unpublished data for 150 mM salt (Z. Bryant) indicate $C_P = 20 \pm 10$ nm.

As for L-DNA, for forces under $\approx$20 pN there is a well-defined torque for the transition from B-DNA to P-DNA, $\tau \approx 40$ pN nm [16,31,34–37,39]. Combining this with the shift in helix rotation angle per base pair of about $\psi_P - \psi_B = 2\pi/3 - 2\pi/10.5 = 1.5$ radians gives a crude estimate of $\epsilon_P = 40 \times 1.5$ pNnm $= 15\,k_B T$.

For 150 mM salt we take $a_P = 1.7a_B$, $\psi_P = 2\pi/3.8 = 1.653469$, $A_P = 15$ nm, $C_P = 25$ nm, and $\epsilon_P = \epsilon_M + 10\,k_B T$. At 150 mM salt, $f = 3$ pN, and $\tau = 5$ pN nm we have $\Phi_P = 11.10\,k_B T$ and $\Phi_{\mathrm{plect},P} = 11.37\,k_B T$.

4. S-DNA

S-DNA has a contour length of roughly 1.7 that of B-DNA, transforming to this form at a well-defined force of 65 pN when under zero torque (twist-unconstrained or "nicked" DNA) [13,14,18]. The extension change of about 0.204 nm/bp at the transition indicates a creation energy per base pair of about 65 pN $\times$ 0.2 nm $= 3.3\,k_B T$. The helix repeat of S has been estimated to be about 35 bp per right-handed turn [16,31,39]. From force-extension measurements the bending persistence length has been estimated to be 15 nm [17]. No data are available for the twist persistence length for S-DNA.

For 150 mM salt we take $a_S = 1.7a_B$, $\psi_S = 2\pi/35 = 0.179519$, $A_S = 12$ nm, $C_S = 20$ nm, and $\epsilon_S = 3.3$ $k_B T$. At 150 mM salt, $f = 3$ pN, and $\tau = 5$ pN nm we have $\Phi_S = 3.506\,k_B T$ and $\Phi_{\mathrm{plect},S} = 3.773\,k_B T$.

5. Q-DNA

Although a left-handed version of P-DNA has been noted to be stereochemically possible [38], essentially nothing is known experimentally about this proposed state. We use $a_Q = 1.7a_B$, $\psi_Q = -2\pi/3.8 = -1.653469$, $A_Q = 15$ nm, $C_Q = 25$ nm, and $\epsilon_Q = \epsilon_M + 11k_B T$ for 150 mM univalent salt, corresponding to essentially a left-handed version of our P-DNA state.

At 150 mM salt, $f = 3$ pN, and $\tau = 5$ pN nm we have $\Phi_Q = 16.13\,k_B T$ and $\Phi_{\mathrm{plect},Q} = 16.41\,k_B T$.
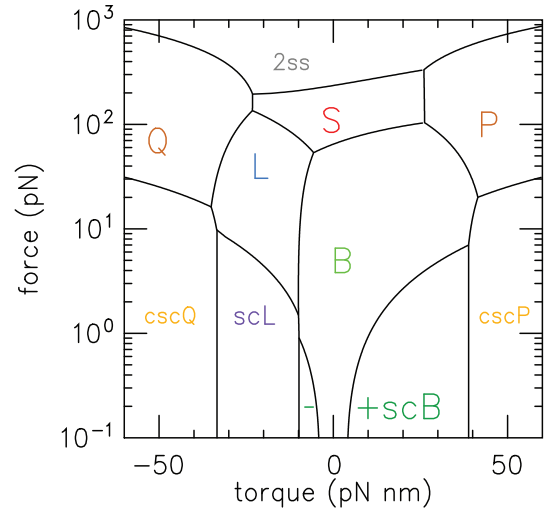

FIG. 4. (Color online) Force-torque phase diagram for unnicked dsDNA under force and torque at 150 mM salt. First-order-like transitions are shown as black lines, with discontinuous changes in linking number and extension occurring as they are crossed.

B. Structure of phase diagram

For the parameters described in Sec. III A, appropriate for 150 mM univalent salt, the overall force-torque phase diagram is shown in Fig. 4. This diagram is computed by finding the minimum free energy state $\Phi_i(f,\tau)$ for each force-torque point.

There are 16 candidate states considered in our theory. Fifteen of them are based on the B, L, S, P, and Q states, each of which can be in extended, inflated-supercoiled (sc) or collapsed-supercoiled (csc) forms. The additional state is the unwound-parallel ssDNA "2ss" state. Of those 16 states, only 10 actually occur as free energy minima for some force-torque combination; cscB, cscL, scP, scQ, and both varieties of supercoiled S (scS and cscS) are never global minima. Supercoiled B- and L-DNA are only found in the inflated (scB) form, while P and Q are only found in the collapsed (cscP and cscQ) forms. We do not find any of the supercoiled states to display inflated-to-collapsed transitions (csc-sc) but that can occur if the parameters differ somewhat (for other salt concentrations for example).

Transitions are indicated by solid lines: Black lines indicate first-order-like transitions at which two states have the same free energy but different linking number densities and, for extended phases, different extensions. Triple points occur where three first-order lines meet (Table II); at these points three phases have equal free energies.

1. B-DNA

At very low forces ($<$0.2 pN) and torques ($|\tau| < k_B T \approx$ 4 pN nm), extended B-DNA is the stable state. When torque reaches $\approx k_B T$, plectonemic supercoiled B becomes stable [3,4,43]. This occurs before the limit of stability of the extended state $\tau = \sqrt{4k_B T A f}$ is reached. The transition is first-order-like with linking number density and extension per base of the "pure" phases changing discontinuously as the B-scB transition is crossed. As one might expect from the

TABLE II. Coordinates of triple points in Fig. 4.

Triple point	τ (pN nm)	f (pN)
B-scB$^+$-cscP	39	7
B-P-cscP	41	20
S-B-P	26	104
S-P-2ss	27	330
B-scB$^-$-scL	-10	0.9
B-L-scL	-10	1.5
L-scL-cscQ	-33	10
L-Q-cscQ	-35	16
L-S-B	-5	54
L-Q-S	-23	160
S-Q-2ss	-23	190

buckling threshold behavior, as force is gradually increased, the B-scB transition torque ($\tau_{\text{B-scB}}^*$) magnitudes gradually rise; see Eq. (17) of Ref. [8].

The discontinuous change in linking number at the B-scB transition at fixed f and τ gives rise to "forbidden regions" in the linking number density-force phase diagram, where a pure phase state is impossible. These are the unlabeled regions of Fig. 5(a). In experiments with fixed linking number and force [Fig. 5(a)], supercoiling of B-DNA is observed as "phase coexistence" of the B and scB states.

The linking number of B-DNA at which it starts to be converted to scB ($\sigma_{\text{B,scB}}^*$) is related to the B-scB coexistence (transition) torque ($\tau_{\text{B-scB}}^*$) via $\sigma_{\text{B,scB}}^* = [a_B/(k_B T \psi_B C_{B,f})]\tau_{\text{B-scB}}^*$,
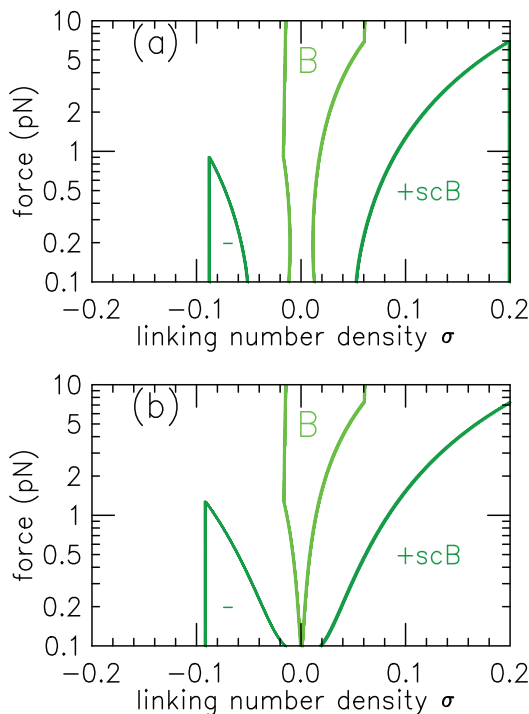

FIG. 5. (Color online) (a) Force-linking number phase diagram for dsDNA for forces below 10 pN and linking number densities with magnitude less than 0.2. (b) Corresponding phase diagram with the entropic term removed; the +scB and $-$scB regions nearly meet and extended B-DNA is nearly eliminated at low forces.
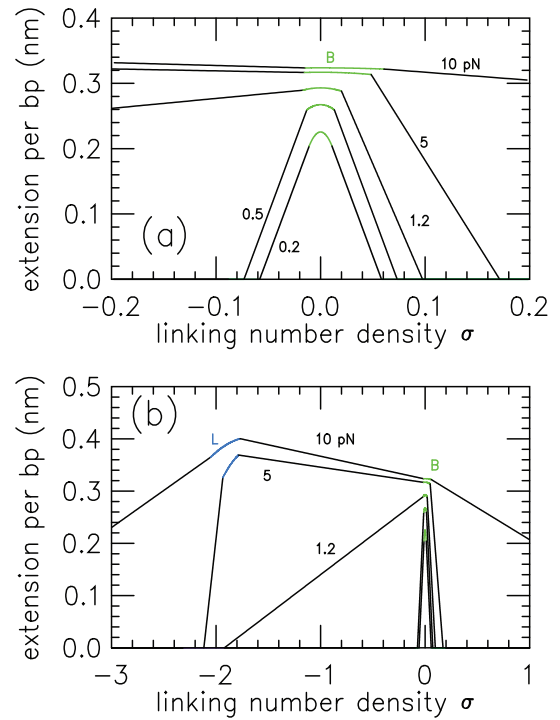

FIG. 6. (Color online) (a) Extension versus linking number for forces of 0.2, 0.5, 1.2, 5, and 10 pN (curves from bottom to top) and linking number densities of magnitude less than 0.2. Black straight line segments indicate coexistence regions while central nonlinear segments indicate pure phases, as marked. For 0.2 and 0.5 pN, the coexistence regions link B to scB (at zero extension). Note the rapid change in slope for negative linking number as force is changed from 0.5 to 1.2 pN; this is due to the B-scB-scL triple point. The coexistence region for 1.2 pN and negative linking number connects B to scL; that for 5 and 10 pN connect B to extended L. (b) Extension versus linking number for forces as in (a) but for a larger range of linking number density from -3 to $+1$. Straight lines indicate coexistence regions while nonlinear regions indicate pure B and L states as marked. For 10 pN the coexistence curve leading off the graph for negative linking number leads to cscQ; that for positive linking number leads to cscP.

where $C_{B,f}$ is the force-dependent twist persistence length of B-DNA. For example, at 0.2 pN, $C_{B,f} \approx 40$ nm, so $|\sigma_{\text{B,scB}}^*| \approx (0.34 \text{ nm} \times 5 \text{ pN nm})/(4 \text{ pN nm} \times 0.6 \text{ rad} \times 40 \text{ nm}) \approx 0.015$. This value of $\sigma_{\text{B,scB}}^*$ corresponds to that seen in Fig. 5(a). The linking number density of the coexisting supercoiled-B state is appreciably larger than $\sigma_{\text{B,scB}}^*$; for 0.2 pN the coexisting scB state has $|\sigma_{\text{scB,B}}^*| \approx 0.05$.

As linking number density of the molecule is increased beyond $\sigma_{\text{B,scB}}^*$, progressively more of the molecule is converted to the scB form, until, finally, when σ reaches $\sigma_{\text{scB,B}}^*$, the molecule becomes entirely of the scB form and of zero extension. This gives rise to a linear variation of extension with linking number as B is converted to scB [Fig. 6(a)], which is an instance of a Maxwell-like coexistence region and may be equivalently described in the linking number-force ensemble [3,4,8,43]. The linear extension-linking number regions correspond to torque plateaus as a function of linking number [Fig. 7(a)].
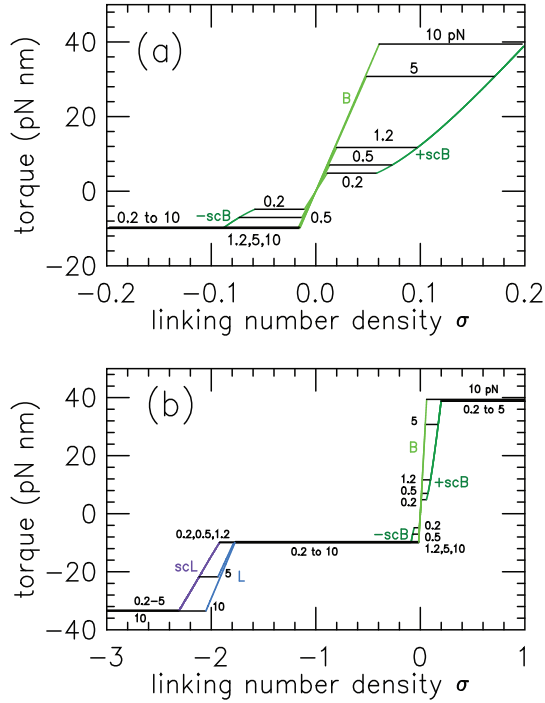
FIG. 7. (Color online) (a) Torque versus linking number for forces of 0.2, 0.5, 2, 5, and 10 pN and linking number densities between −0.2 and 0.2. Horizontal black lines indicate coexistence regions; nonhorizontal segments indicate pure states as marked. (b) Torque versus linking number as for (a) but for linking number densities between −3 and +1.

This general scheme of state coexistence is common to all of the first-order-like transitions of the model. We also note that at the B-scB transition, there is a small discontinuous jump in extension observed in experiments on finite-length molecules corresponding to the initial "buckling" transition [32]. This is not included in the present theory but could be added following methods used previously [9,57,58] along with multiple-plectoneme fluctuations [9,59].

We note that at low forces, there is a clear separation of positive and negative linking number scB states [one might even label these as different states, e.g., +scB and −scB, given their reversed chiralities and separation by phase boundaries; see Fig. 5(a)]. This separation is driven largely by the entropic confinement free energy for the supercoil (see Eq. (11) and Refs. [3,4]) which generates a transition at a solidly nonzero τ and σ for the lowest forces in Fig. 4.

If one removes the entropic confinement term from the model, the low-force behavior of the B-scB transitions is strongly modified, with the two scB states moved nearer together [Fig. 5(b); for symmetry reasons there must always be at least one first-order transition separating +scB and −scB since one cannot convert one sign of plectoneme to the other without passing through a chiral random coil [4] or, at nonzero force, the extended state]. Given this, careful experimental determination of the B-scB transition linking number or torque values could be used to estimate the numerical prefactor of the confinement entropy term in (9), which is somewhat of a theoretical loose end: Imposing a "hard" confinement constraint is problematic even for the problem

of a polymer in a fixed-geometry tube, and in a plectonemic supercoil deciding exactly what the constraint should be is not straightforward beyond the level of scaling of the effective potential [3,4].

2. L-DNA

After creation of entirely negatively supercoiled B (still considering force ≈0.2 pN in Fig. 4), the molecule can be further unwound to have $\sigma < \sigma^*_{scB,B}$, generating torques $< \tau^*_{B\text{-}scB}$ [Fig. 7(b)]. As stronger unwinding torques are introduced, one might imagine the "inflated" scB state, which has $R > R_{0,B} = 1$ nm, to convert to a collapsed cscB state. But this is pre-empted by a transition to "inflated" scL-DNA, which becomes the most stable state for a torque slightly larger than −10 pN nm. This state has a linking number density near to $\sigma = -2$.

At larger forces, above the B-scB-scL triple point but below the B-scL-L triple point (between about 1 and 2 pN), with progressive underwinding one passes from B to scL by a coexistence region. This transition is often described as "melting" by unwinding and is characterized by a nearly flat extension [30,60] when plotted over a relatively small σ scale [typically $|\sigma| < 0.1$; see the 1.2 pN curve in Fig. 6(a)]. In fact, the extension curve is not flat but has a downward slope visible on a wider σ range [Fig. 6(b)], finally reaching zero extension for $\sigma \approx -2$, characteristic of the pure scL state.[2] The transition to scL generates a constant-torque plateau at ≈−10 pN nm [Figs. 7(a) and 7(b)], observed experimentally [36].

Starting from scL, as force is increased, one reaches a point where extended L becomes stable (Fig. 4). This transition is first order, displaying coexisting-state behavior similar to that for the B-scB transition. Experimentally, this is most easily observed by gradually reducing linking number starting from the relaxed state and measuring extension and torque above the B-scL-L triple point. The triple point is characterized by a large change in slope of the extension versus σ curve with a small increment in force [Fig. 6(a), compare the 0.5 and 1.2 pN curves].

For forces slightly above the B-scL-L triple point ($f > 2$ pN), the model gives an extension versus linking number curve starting with extended B-DNA near $\sigma = 0$, a coexistence region to extended L-DNA [linear slope on 5 pN curve of Fig. 6(b)], followed by a nonlinear variation of extension as torque on extended L builds up and then a second linear dependence of extension on σ occurs as scL is formed [5 pN curve for Fig. 6(b)]. Zero extension is reached slightly beyond $\sigma = -2.1$, when the entire molecule becomes scL.

This two-triple-point scenario is supported by the experimental data of Sheinin et al. [36]. Figure 8(a) shows extensions versus linking number, while Fig. 8(b) shows torque versus linking number for the series of forces studied in Ref. [36]. These plots should be compared with Figs. 1(a) and 1(b) and Fig. 3 from Ref. [36]. For 1.2 pN, one sees a transition with

---

[2]One should distinguish this characteristic value $\sigma \approx -2$, occurring at torque $\tau \simeq -10$ pN nm, from the preferred linking number density $\sigma_L = -1.66$, defined for zero torque.
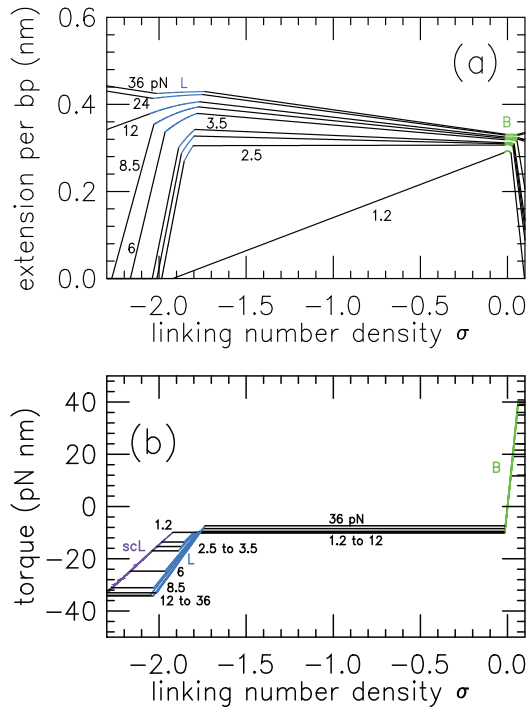
FIG. 8. (Color online) (a) Extension versus linking number for forces of 1.2, 2.5, 3.0, 3.5, 6, 8.5, 12, 24, and 36 pN as studied in Ref. [36] (curves for progressively increasing forces have progressively higher extensions). The 1.2-pN curve shows a transition from B to scL; the 2.5- to 8.5-pN curves show B-L and L-scL transitions; the 12-pN curve shows B-L and L-scQ transitions; finally, the 24- and 36-pN curves show B-L and L-Q transitions. (b) Torque versus linking number corresponding to the forces in (a). Note that the torque plateau levels are not monotonically ordered with force.

underwinding from B to scL, resulting in a gradual reduction in extension to zero as σ is decreased from -0.05 to -2, accompanied by a torque plateau at ≈ 10 pN nm. For larger forces (2.5 to 8.5 pN) a transition from B to extended L occurs, resulting in an extension which shows a "flat-top" response out to $\sigma \approx -2$ accompanied by a torque plateau again near 10 pN nm. Then, scL is formed, and the extension rapidly drops as σ is increased beyond -2.

Sheinin *et al.* [36] also measured the extension versus force for L-DNA at the L end of the B-L torque plateaus, where one has converted the molecule to the "pure" L form. This corresponds to the L-DNA extension along the B-L phase boundary of Fig. 4 between the scL-L-B and L-B-S triple points. This force-extension relation is plotted in Fig. 9 along with the experimental measurements of Sheinin *et al.* [36]; there is good agreement of the model and experimental data. Note that this force-extension curve is that of L-DNA under appreciable negative torque varying from ≈ -10 pN nm for low forces to ≈ -5 pN nm for large forces.

For $\sigma < -2$ the apparent ≈ -40-pN nm torque plateau observed by Sheinin *et al.*, which is also present in Fig. 7(b), suggests the existence of an additional state [36]. Discussion of this is deferred as this involves the hypothesized Q state (termed "LP-DNA" in Ref. [36]).
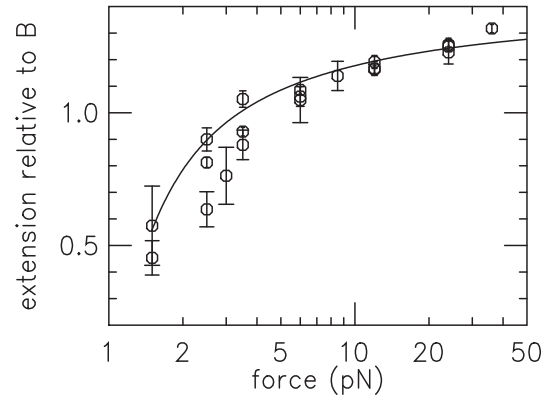

FIG. 9. Extension versus force for L-DNA, along the B-L transition line of Fig. 4 along with the corresponding experimental data of Sheinin *et al.* [36].

3. P-DNA

We now move to the positive-torque side of Fig. 4. For few-pN forces and for increasing positive torques, the first states other than B or scB that are met are based on P-DNA. At low forces (<20 pN) torques of roughly 40 pN nm lead to a transition from either scB or B to cscP, depending on whether one is below or above the B-scB-cscP triple point (the upper limit of the scB state) at about 7 pN. If one is below the triple point, the scB-cscP transition encountered with increasing positive torque involves no change in extension (both states have zero extension) but does involve a change in torque [5-pN curves; Figs. 10(a)–10(b)]. Notably, we find that supercoiled P is always collapsed, with the two P double helices driven to close contact by the large torques.

Just above the B-scB-cscP triple point, the extension shows a dramatic change; the B-cscP coexistence region terminates at the large value of linking number associated with the cscP state, $\sigma \approx +2.8$.[3] Note that this coexistence region, viewed on a smaller σ scale [10-pN curve, Fig. 6(a)] appears as a nearly flat extension versus linking number response.

A second higher-force B-P-cscP triple point is not far away, at roughly 20 pN; above this triple point B changes to P as torque is increased. Now, one sees an increase in extension as the molecule is overwound [25-pN curve, Fig. 10(b)], followed by formation of cscP (reduction in extension). Notably, as force is increased beyond 30 pN, there is a reduction in the torque at the B-P transition, essentially due to the contribution of work done by the force to reducing the work needed from torque to create the P state. This effect has been observed by Bryant *et al.* [31], who found that P was created at a torque of ≈ 35 pN nm for DNA under 45-pN tension, smaller than the ≈ 42 pN nm observed to be needed to create P at lower forces [36].

4. Q-DNA

Having discussed how P appears in the phase diagram for positive torques, we examine the opposite side of the phase diagram where the strongly left-handed Q state is

---

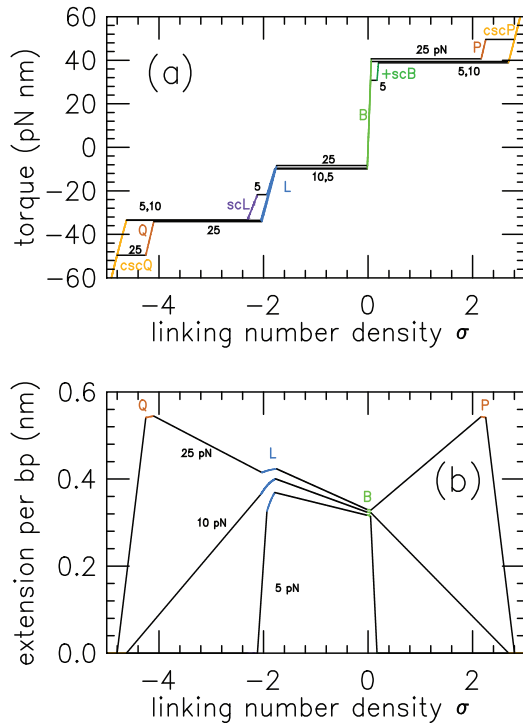[3]As for L-DNA, this value should not be confused with $\sigma_P = 1.8$.

FIG. 10. (Color online) (a) Torque versus linking number for forces of 5, 10, and 25 pN for linking number densities between −5 and +3. Horizontal line segments indicate coexistence regions; nonhorizonal segments indicate pure states as marked. (b) Extension versus linking number for forces of 5, 10, and 25 pN for linking number densities between −5 and +3.

found. Qualitatively, many of the properties of the scB-B-cscP-P transitions apply to transitions to Q, except that the transitions now involve scL-L-cscQ-Q (as for P, only the collapsed supercoiled Q state appears). The torque required for generation of Q is approximately −35 pN nm, and we have a scL-cscQ-L triple point just below 20 pN, followed by a cscQ-Q-L triple point several pN above that.

Torque and extension versus linking number associated with the transitions from L to Q and cscQ are shown on the left side of Fig. 10. A torque plateau at about −35 pN nm is associated with creation of the Q state [Fig. 10(b)]; this is apparent in the experimental data of Sheinin *et al.* [36] for $\sigma < -2$. At 5 pN, one is below the scL-L-cscQ triple point, so the extension has already been zeroed by creation pure scL, where $\sigma \approx -2$, but one can in principle imagine measuring the appearance of the −35-pN nm torque plateau as scL converts to cscQ.

Above the scL-L-cscQ triple point but below the L-cscQ-Q triple point (≈ 10 pN), a different behavior is observed, whereby L converts to the zero-length cscQ state, with a σ near −5 [10-pN curve, Fig. 10(b)]. The experimental signature of this is a drastic change in slope of the extension-linking number curve [compare 5- and 10-pN curves in Fig. 6(b) for $\sigma < -2$; also see similar extension-linking number curves for forces above 10 pN in Fig. 8(a)]. This is apparent in the data of Sheinin *et al.*, who observe a drastic change in slope of the extension-linking number curves with increasing force (Fig. 1 of Ref. [36]).

For larger forces (25 pN, Fig. 10) above the L-cscQ-Q triple point, yet another behavior is observed: One sees an increase in extension with σ as extended Q is created, followed by extension dropping to zero as cscQ is formed. The extension drops to zero at the linking number density associated with pure cscQ, at $\sigma \approx -5$.

Both the drastic change in slope of the extension-linking number response as one passes through the scL-L-cscQ triple point and the −35-pN nm plateau for $\sigma < -2$ in the torque-linking number response (both observed by Sheinin *et al.* [36]) strongly suggest the appearance of the cscQ state. The main discrepancy between the current model and the measurements of Sheinin *et al.* [36] is the lack of signature of the even higher-force L-cscQ-Q triple point, which causes an extension increase for $\sigma < -2$ in the model. The experimental data show a flattening but not quite an upturn in extension curves (Fig. 1(a), Ref. [36]).

5. S-DNA and parallel ssDNAs

At high forces there are two more states which are well known from zero-torque high-force studies. As one ascents at zero torque, B- gives way to S-DNA at about 65 pN. Then, at even larger forces ≈250 pN, S-DNA becomes unstable to the formation of parallel-strand "2ss" melted DNA, which in our model has all its twist expelled. At these very high forces, one finds mainly the 2ss state, despite the large free energy cost of setting the twist to zero, thanks to the large free energy gain associated with fully extending the ssDNA backbones.

6. Force-linking number phase diagram

Figure 11 shows the phase diagram in force-linking number coordinates. The various "pure states" are as indicated and form a number of enclosed regions in the f-σ plane. The blank regions between the pure state regions are coexistence regions, in which pure states are forbidden. One can construct constant-force "tie lines" that connect the edges of the pure states; these lines represent the mixed states that can be seen
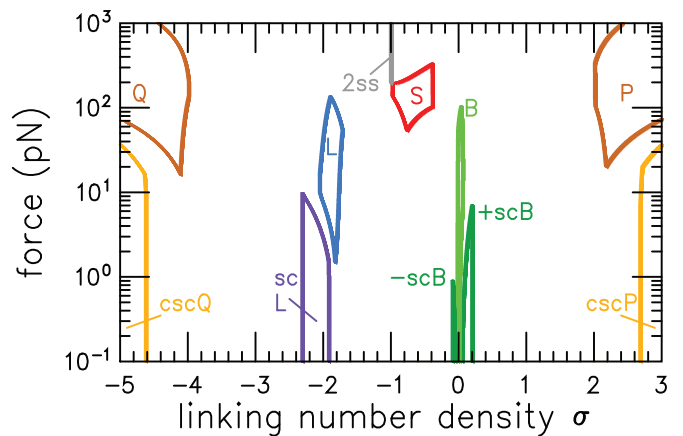

FIG. 11. (Color online) Force-linking number density phase diagram on wide f and σ scale. Enclosed labeled areas are the pure states; blank areas are coexistence regions. Coexistence ("tie") lines stretch horizontally (constant-f) from boundaries of the pure state regions. Triple points occur when a tie line is tangent to the top or bottom of a pure state region.

to minimize free energy in the f-σ ensemble [3,4,43] via the analog of the "Maxwell construction" familiar from theories of liquid-gas phase coexistence.

The triple points of the force-torque phase diagram (Fig. 4) correspond to forces in the force-linking number phase diagram (Fig. 11) at which tie lines between two states are tangent to a third pure state region. These tangent points correspond to the cusplike minima and maxima of the pure phases of Fig. 11. For example, the S-B-P triple point at about 100 pN and +25 pN nm in Fig. 4 corresponds to the S-P tie line at 100 pN in Fig. 11, which is tangent to the upper tip of the pure B region. A second example is the B-L-S triple point, which is tangent to the lowest point of the pure S region of Fig. 11. In this way, all the triple points of Fig. 4 can be located in the force-linking number phase diagram.

Note that the 2ss state has contracted to a narrow region in the f-σ phase diagram. This is a result of the lack of a twist modulus term in (22).

7. Comparison with results of Léger et al.

A second experimental data set that we compare our model with is that of Léger *et al.* [16,39]. These data are composed of force-extension curves for a series of fixed σ ranging from roughly -1 to $+1$ (rather than the extension-linking number curves of Sheinin *et al.* [36]). Figure 12 show force-extension curves calculated for (negative [Fig. 12(a)] and positive [Fig. 12(b)] σ values for direct comparison with Figs. 1 and 2 of Ref. [39].

Figures 12(a) and 12(b) include the zero-torque force-extension curve, which corresponds to the elasticity of a nicked (torsionally unconstrained) DNA (dashed curve). The $\tau = 0$ result shows a single prominent plateau at about 65 pN, corresponding to the B-S transition of Fig. 4.

The curves at fixed linking number (σ) can be understood by reference to the force-linking number phase diagram (Fig. 11). In Fig. 12(a), the $\sigma = 0$ curve corresponds to a path at increasing force along the vertical line $\sigma = 0$ in Fig. 11; this curve passes through the pure B-DNA region but then reaches the end of it at around 70 pN, causing a slight kink in the force-extension curve as S starts to be created. Then, at 100 pN, one reaches the S-B-P triple point and a prominent plateau is observed as the B-S mixture is replaced by a mixture of S and P at higher forces. At $\sigma = -0.83$, one has a transition from B to essentially pure S at 50 pN. These features have been observed experimentally [16,39].

As the molecule is underwound ($\sigma \approx -0.12$ to -0.36), one leaves the pure B region at low forces with the result that one has a mixture of B and L at moderate forces (10 pN); finally, one reaches the B-L-S triple point at about 50 pN, leading to replacement of the B-L mixture with a B-S mixture at higher forces at the 50-pN plateau. At yet higher forces one reaches the B-P-S triple point and the 100-pN plateau. As the molecule is increasingly underwound, the 50-pN plateau gradually grows as the 100-pN plateau shrinks, corresponding to a gradual increase in the amount of S and P relative to B. The 100-pN plateau disappears for $\sigma < -0.4$ since one ends up inside the pure S phase at high forces.

For overwinding [Fig. 12(b)] one sees even richer behavior. At low force, the rather robust +scB state is present until forces
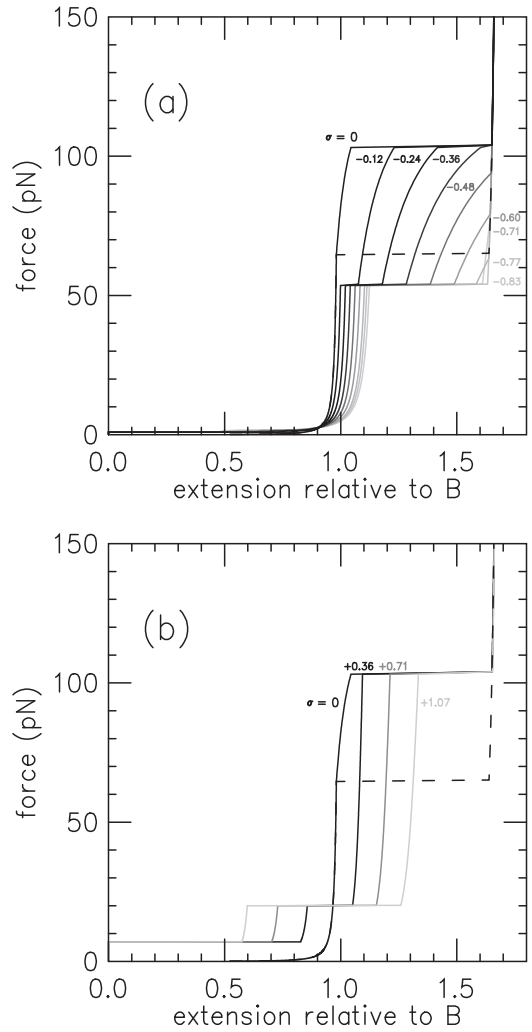

FIG. 12. Force-extension curves for DNA held at fixed linking number at the same σ values studied in Ref. [39]. For comparison, dashed curves indicate force-extension response for DNA with zero torque and variable σ, which shows a prominent plateau at 65 pN corresponding to the B-S transition. (a) Underwinding: For $\sigma = 0$ a single plateau occurs at $\approx$100 pN corresponding to coexistence of B with a mixture of P and S at the B-P-S triple point. As the molecule is wound to $\sigma < 0$, a new plateau at $\approx$50 pN associated with the B-L-S triple point gradually replaces the 100-pN plateau. (b) Overwinding: As the molecule is wound to $\sigma > 0$, one observes the appearance of a gradually broadening plateau at $\approx$20 pN, corresponding to conversion of a B-cscP mixture to a B-P mixture, as the B-P-cscP triple point is passed.

of about 8 pN, leading to the initial low-force plateau. Then, for overwinding of $\sigma = +0.36$, a plateau at 20 pN is observed, at the point where the B-P-cscP triple point is reached (the cusp at the bottom of the pure P state region in Fig. 11). This 20-pN plateau broadens as one further overwinds the molecule. At higher forces, one reaches the B-P-S triple point and the 100-pN plateau, which gradually is reduced in width as the molecule is increasingly overwound.

The experiments of Leger *et al.* for underwound DNA had a limit of underwinding of $\sigma \approx -0.83$, essentially inside the rather broad L-B coexistence region and the pure S region.

It would be quite interesting to have additional experimental studies for larger underwinding ($\sigma \approx -3$) where one could look for corresponding signatures of the Q state.

At higher forces than the 150-pN limit of Ref. [39] it would be in principle possible to detect the even higher-force triple point behavior; this may be difficult since all the high-force states (2ss, S, P) have approximately the same lengths.

IV. CONCLUSIONS

This paper has presented a theoretical model of structural transitions of dsDNA driven by tensile and torsional stress. The approach has been to consider the various different states as semiflexible polymers, each with characteristic contour lengths per base pair, double helix diameters, bending stiffnesses, twist angles per base pair, and twisting stiffnesses, based, when possible, on experimental data [16,31,36,38,39]. Our model considers the well-established and distinct B, P, L, S, and unpaired-ssDNA states, plus Q, a hypothetical but plausible [38] left-handed version of the P state. The global phase diagram, force-extension curves, and extension-linking number curves are in overall good agreement with available experimental data [16,31,36,39] (we note the similarities of the phase boundaries reported in Fig. 4 of Ref. [31] and Fig. S3 of Ref. [36] to Fig. 4 of this paper). In this section we discuss the main new results of this paper, and we also point out several areas where there remain open questions and where the present theory needs further development.

A. Supercoiled states and collapsed plectonemes

Supercoiled versions of the B, P, L, S, and Q states are computed using models for plectonemic interwinding similar to those developed for B-DNA [4–9], which take as their sole inputs the same structural and elastic data used for the extended states. For the first time it has been shown that such a model can provide a reasonable global phase diagram, with supercoiled states present at low forces and extended states present at higher ones. Notably, supercoiled S-DNA does not occur in our phase diagram.

A second new element of the computations of this paper is the elucidation of two distinct types of plectonemic supercoiling. The first possibility are plectonemes which are "inflated" by a combination of electrostatic and entropic repulsions (similar to plectonemic B-DNA states discussed in prior works [4–9]). The second type of plectoneme is "collapsed," with tightly juxtaposed double helices (first reported in Ref. [7]). The collapsed state occurs when elastic forces favoring tightening of a plectoneme can entirely overcome opposing repulsive forces. In this paper we have presented the first detailed discussion of this effect.

We find that at physiological salt levels (150 mM NaCl), the B and L states only form inflated supercoils; on the other hand, P and Q are only found as collapsed supercoils. The general rule appears to be that collapsed plectonemes require a large amount of torsional stress. Another approach to generation of collapsed supercoils might be to make the double helix *thicker*. This could occur for protein-DNA complexes where DNA-binding proteins are bound in arrays along B-DNA. It may well be that chromatin fibers under torsional stress form collapsed

plectonemic supercoils, due to their thickness of 10 to 30 nm. To see this, note that if R_0 is set to 5 nm in Fig. 2 (the radius of a nucleosome), one would have collapsed plectonemes beyond very low torques for 150 mM salt, suggesting a generally collapsed plectonemic state for chromatin under physiological salt conditions. This may be relevant to gene expression control mechanisms which require physical contact of two chromatin loci in the same supercoiled loop domain.

Interestingly, for naked DNA we did not find any case where a given state supercoils first into an inflated state which subsequently collapses. Such transitions are possible and can be either discontinuous or continuous (first- or second-order-like). It is conceivable that one could tune such transitions into existence by varying salt concentration or again by use of DNA-binding proteins to increase the effective B-DNA diameter.

B. Triple points

A main feature of the force-torque phase diagram (Fig. 4) is the appearance of a number of triple points, values of force and torque where three states coexist. Perhaps the best-studied example of this is the rather low-force ($\approx$1 pN) B-scB-scL triple point, which gives rise to a rapid change in slope of the extension-linking number curves as one passes through it [Fig. 6(a)]. This rapid change in slope of the coexistence parts of the extension-linking number curves is a general diagnostic for the triple points; see Fig. 13. One can also find the signature of a triple point in the form of force plateaus along force-extension curves at a fixed linking number [16,39].
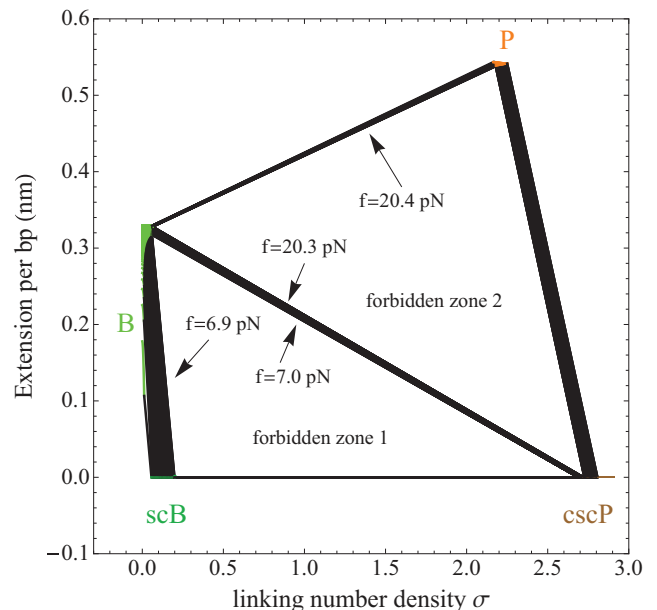

FIG. 13. (Color online) Extension-linking number curves for forces $f = 0.1, 0.2, 0.3, \ldots, 25$ pN and positive supercoiling ratio. Large parts of the diagram, called "forbidden zones," stay empty as no curve reaches them, due to the rapid change in slope at the triple points. The limiting value of forces at the boundaries of the "forbidden zones," $f \simeq 7$ pN and $f \simeq 20$ pN, yield values for forces at triple points.

Experimental evidence exists for a number of the triple points in Fig. 4 (B-scB-scL, B-scL-L, B-scB-cscP, B, cscP-P, B-S-P [16,31,34,36,38,39]) but a number of others still await clear experimental verification (scL-cscQ-L, cscQ-Q-L, B-L-S plus the triple points involving the unpaired ssDNA state). The results of this paper can provide a guide for searching for these previously unobserved triple points.

C. L-DNA

We have followed Sheinin *et al.* [36] by introducing a semiflexible polymer model to describe the L state. This state is thought to be partially stress-melted, and other authors have suggested that it might be a mixture of left-handed Z-like DNA and left-twisted molten DNA [37]. Nevertheless, it does behave as if it has a well-defined helix repeat of between 10 and 15 bp ($\sigma \approx -2$), with a force-extension response much better modeled by a semiflexible polymer than by completely denatured DNA. We have extended the Sheinin approach by including a supercoiled L state based on the same microscopic parameters as the extended state, which leads to a reasonable description of experimental data.

We have used a substantially longer persistence length ($A_L = 7$ nm rather than the ≈ 3 nm of Sheinin *et al.* [36]) to fit the experimental results as well as possible. The relatively large value of A_L was also used (more precisely a relatively large value of A_L/C_L) because of the behavior of the model for plectonemic supercoiling used here. For low persistence length values, the linear limit of stability of the extended state ($4k_B T A f = \tau^2$ [42]) is reached *before* the free energy of the plectoneme actually drops below that of the extended state. The extended state can therefore *disappear* before the plectoneme becomes globally stable.[4] Theories with mean-field-like single-plectoneme-domain supercoiled states are incomplete: Many-plectoneme or many-chiral-"curl" states [9,59] are likely to occur as an intermediate between the high-force extended state and the low-force large-plectoneme-domain states for polymers with low A/C ratios.

The use of such many-curl or many-plectoneme states for B and L (and the other states) together is significantly more complicated than the simple mean-field-like model used here and will be discussed in a future paper. However, we can anticipate a broadening of transitions between scB, B, scL, and L due to the appearance of many small plectonemic or loop domains near the L-scL boundary. Supercoiling-domain fluctuation effects [9], mixing of domains of different states [16], and, of course, sequence-disorder effects are all likely to contribute to the smearing of the sharp transitions that occur in the simple mean-field-like description of this paper.

Given the increased importance of many-plectoneme states at low salt concentration [9] we also defer discussion of salt effects to a future paper. The present model can be used to crudely estimate salt effects, and we note that the general trends are towards destabilization of the plectonemic states at

low salt (e.g., 10 mM NaCl) and towards stabilization of the plectonemic states at high salt (e.g., 500 mM NaCl).

We note that at physiological salt (150 mM NaCl) the S state is always intermediate between B-DNA and the unpaired-ssDNA state. This result holds for unnicked DNA; for DNA with nicks one strand can "unpeel" from the other given sufficient destabilization of the double helix (low salt or elevated temperature) [18,22,23]. It may also be possible, at low salt or elevated temperature, for transitions to occur for *unnicked* molecules from B to strand-separated forms. In some sense, this occurs as torque is increased, since L-DNA is thought to be at least partially base unpaired [37].

D. Q-DNA

It is quite clear that a highly underwound state other than L-DNA exists, due to the appearance of a $\approx$40-pN nm plateau for $\sigma < -2$ in torque-linking number data of Sheinin *et al.* (Fig. 1(a) of Ref. [36]; note also the rapid variation of the extension-linking number response with increasing force beyond about 10 pN). Our model produces this behavior via L-cscQ transitions, following the suggestion of Sheinin *et al.* that there should be a new, left-handed analog of P-DNA.

A discrepancy between the model and results of Sheinin *et al.* is the lack of clear experimental observation of the effect of the L-cscQ-Q triple point near 20 pN, which causes an extension increase for $\sigma < -2$ for large forces in the model. The lack of observation of this effect for forces up to 36 pN might be due to inaccuracy of the location of the Q-cscQ-L triple point in the present theory; our knowledge of properties of the Q state are far poorer than for the other states in the model.

Alternately, the Q state may have appreciable contour-length extensibility; in the present theory all the states have fixed contour lengths to keep the numbers of parameters in the theory under control. Third, it is possible that Q-DNA, with exposed bases, might have a tendency to stick to itself, appreciably lowering the free energy of the cscQ phase and allowing it to persist to higher forces than found in this paper (adding this effect to the model is simple; one just shifts the free energy of the cscQ state).

A fourth possibility is, similar to the possibility mentioned above for L-DNA, that there might be some additional state intermediate between plectonemic and extended forms such as a series of tight loops, which might give the Q state a wide range of contour-length extensibility for forces near the Q-scQ boundary. In any case, experiments measuring the extension-σ curve for higher forces than those used in Ref. [36] are essential to determine whether there is an extension increase as $\sigma \rightarrow -5$, which would reveal the extended Q state.

When one looks at the phase diagrams (Figs. 4 and 11) it is apparent that L and Q DNA are in some sense distorted mirror images of B and P DNA. B and L have $\approx \pm 10$-bp helix repeats (defined by base-pairing geometry for dsDNA) while L and Q have $\approx \pm 2.6$-bp repeats (defined by steric effects limiting the maximum linking number possible [38]). This relation between the states gives the phase diagrams an approximate left-right symmetry around zero torque (Fig. 4) and around Lk = 0 or $\sigma = -1$ (Fig. 11). From this point of view the high-force S and 2ss states are self-symmetric, being found close to $\tau = 0$ and $\sigma = -1$.

---

[4]With the present value of $A_L = 7$ nm this does indeed happen in a small region near the cscQ-scL-L triple point.
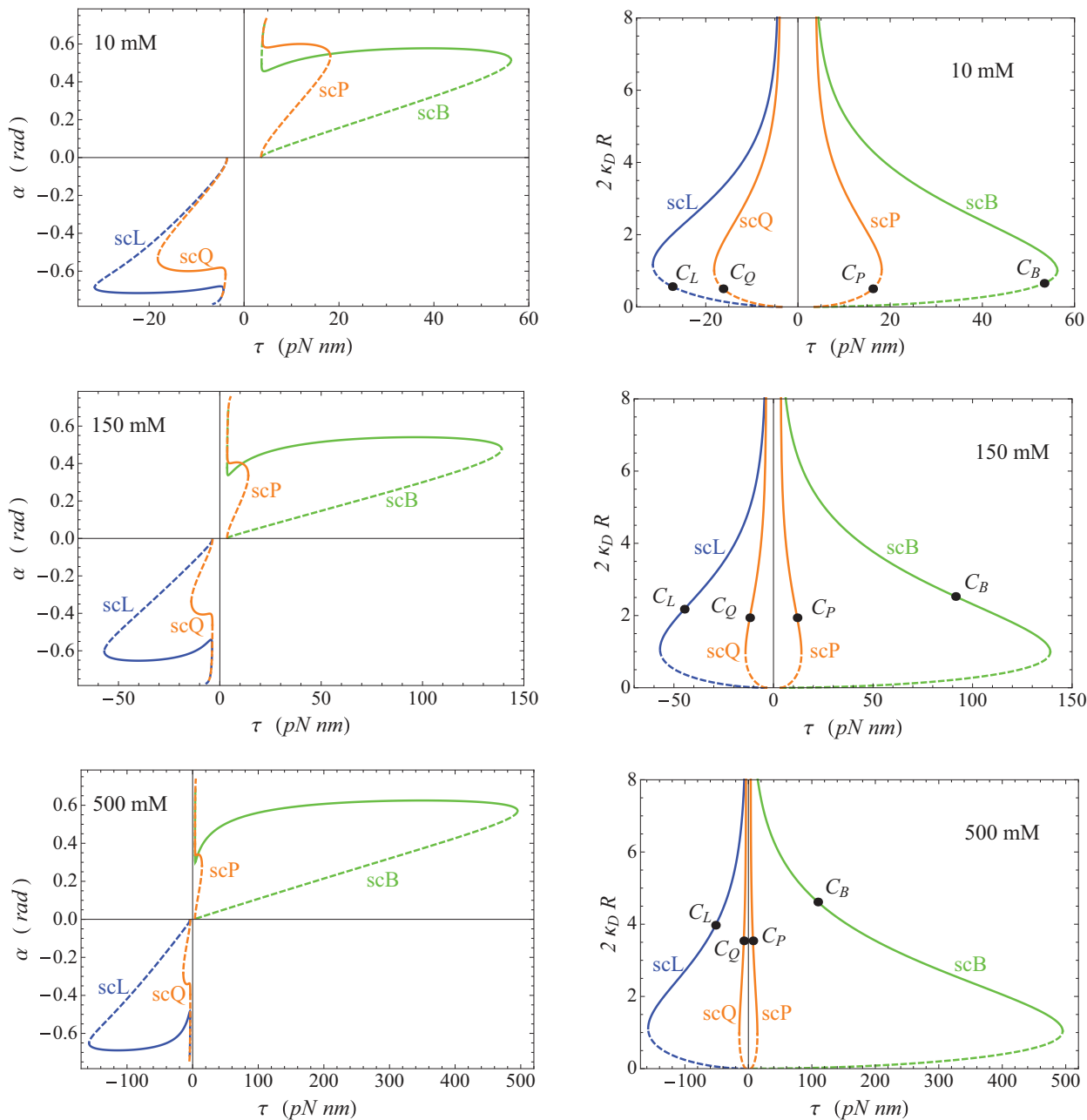
FIG. 14. (Color online) Solution of the system (13) with both electrostatic (10) and entropic terms (11) in the interaction energy for salt concentrations 10, 150, and 500 mM. Solid curves indicate stable solutions; dashed curves indicate unstable solutions.

Of course, this symmetry is broken, with the B state being the lowest free energy state for unstressed molecules; this explicit breaking of chiral symmetry may reflect evolutionary history, e.g., the accidental choice of particular enantiomers as elements of protonucleic acids which subsequently biased selection of a particular chirality for B-DNA. The high-force S and 2ss states are found essentially on the line of symmetry ($\tau = 0$ and $\sigma = -1$).

E. Final comments

All of the non-B states discussed in this paper have double-helix secondary structure disrupted to some degree.

The L state is likely partially strand separated, but it does retain some double-helix-like character, possibly via partial retention of base pairing in GC-rich regions. The P and Q states result from complete loss of base pairing and tight wrapping of the covalently bonded sugar-phosphate backbones around one another. The S state is likely to be partially unstacked; the highest-force 2ss state is, of course, fully strand separated.

It might be possible to construct a more comprehensive model that deals with all these alternative dsDNA states based solely on base pairing, nonspecific adhesion, and steric interactions between the two ssDNAs inside them. This will be challenging given the peculiar polymer elasticity of ssDNA [50–54] and of the fully unpaired state [18] but it might lead
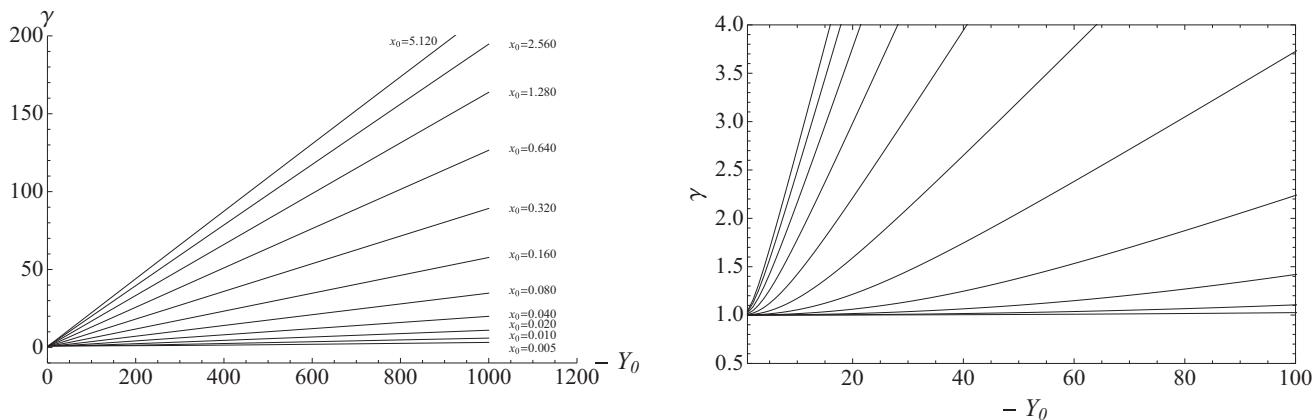
FIG. 15. Values of the scaling parameter γ as function of $-Y_0$ for 11 different values of x_0. Numeric data are provided in the Supplemental Material [64].

to further understanding of the relationships among L, P, Q, and ssDNA. In such an endeavor one must keep in mind the peculiar entropic twist elasticity of braided flexible polymers, characterized by a logarithmically divergent braiding twist modulus, and a consequent tendency towards "braiding phase separation" [55,56].

APPENDIX A: SALT DEPENDENCE OF R AND α

This appendix shows how the solution curves $R = R(\tau)$ and $\alpha = \alpha(\tau)$ vary as the salt concentration is changed. System (13), with both electrostatic (10) and entropic terms (11) in the interaction energy, is solved iteratively for varying τ values. The curves $R = R(\tau)$ and $\alpha = \alpha(\tau)$ are plotted in Fig. 14 for salt concentrations 10, 150, and 500 mM.

APPENDIX B: COMPUTATION OF EFFECTIVE CHARGE

This appendix describes how we compute the effective charge $e\,\nu$, following the approach of Stigter [45]. We seek the electrostatic potential about a charged cylinder immersed in a electrolyte solution. This potential decreases with the distance R from the cylindrical axis. The effective charge $e\,\nu$ is defined in a such a way that the long range ($R\kappa_D \gg 1$) Debye-Hückel

potential, solution of the linear Poisson-Boltzmann equation, matches the $R\kappa_D \gg 1$ asymptotics of the Gouy potential, solution of the nonlinear Poisson-Boltzmann equation [45]. The effective charge $e\,\nu$ is defined with

$$\nu = \frac{1}{b}\,\frac{1}{\gamma(x_0, y_0)}\,\frac{1}{x_0 K_1(x_0)}, \tag{B1}$$

where b is the charge spacing ($b = 0.17$ nm for B-DNA) and $= K_i(\cdot)$ is the ith modified Bessel function of the second kind. The scaling parameter γ has been introduced in Ref. [45] as a function of $x_0 = \rho\kappa_D$, where $1/\kappa_D$ is the Debye length, ρ the radius of the charged cylinder ($\rho = 1$ nm for B-DNA), and $y_0 = y(x_0)$ the potential on the cylinder. For the DNA molecule this potential y_0 is *a priori* an unknown, and the surface charge is the given quantity. Using Gauss flux theorem, we evaluate the electric field $Y_0 = y'(x_0)$ on the cylinder to be $Y_0 = -2L_B/(b\,x_0)$, where L_B is the Bjerrum length. For example, B-DNA at 296.5 K in univalent 150 mM salt has $x_0 = 1.26$ and $Y_0 = -6.55$. We then tabulate the function $\gamma = \gamma(x_0, Y_0)$ and choose the ranges for x_0 and Y_0 in such way that all DNA phases are covered. As for P-DNA, where $\rho = 0.15$ nm and $b = 1.7 \times 0.17$ nm, we have $Y_0 = -239$ at 5 mM, we use 1000 values for $-Y_0$ in (0; 1000). As for B-DNA at 1000 mM we have $x_0 = 3.3$, we use 11 values for x_0: $0.005, 0.01, 0.02, \ldots, 5.12$. We interpolate γ from these 11000 values each time we need to compute ν.

For B- and L-DNA ρ was taken to be equal to $R_{0,i}$ ($\rho_B = 1$ nm and $\rho_L = 1/\sqrt{1.35}$ nm) and we took $\rho = 0.15$ nm for Q- and P-DNA. The charge spacing was taken to be $b = a_i/2$. Values for ν are reported in Table I and compare well with prior estimations [61,62], see also Ref. [63].

[1] P. J. Hagerman, Annu. Rev. Biophys. Biophys. Chem. **17**, 265 (1988).

[2] J. F. Marko and E. D. Siggia, Macromolecules **28**, 8759 (1995).

[3] J. F. Marko and E. D. Siggia, Science **265**, 506 (1994).

[4] J. F. Marko and E. D. Siggia, Phys. Rev. E **52**, 2912 (1995).

[5] S. Neukirch, Phys. Rev. Lett. **93**, 198107 (2004).

[6] N. Clauvelin, B. Audoly, and S. Neukirch, Macromolecules **41**, 4479 (2008).

[7] N. Clauvelin, B. Audoly, and S. Neukirch, Biophys. J. **96**, 3716 (2009).

[8] S. Neukirch and J. F. Marko, Phys. Rev. Lett. **106**, 138104 (2011).

[9] J. F. Marko and S. Neukirch, Phys. Rev. E **85**, 011908 (2012).

[10] T. E. Cloutier and J. Widom, Mol. Cell **14**, 355 (2004).

[11] Q. Du, A. Kotlyar, and A. Vologodskii, Nucl. Acids Res. **36**, 1120 (2008).

[12] J. S. Lucia, H. T. Allawi, and A. Seneviratne, Biochemistry **35**, 3555 (1996).

[13] P. Cluzel, A. Lebrun, C. Heller, R. Lavery, J.-L. Viovy, D. Chatenay, and F. Caron, Science **271**, 792 (1996).

[14] S. Smith, Y. Cui, and C. Bustamante, Science **271**, 795 (1996).

[15] J. F. Marko, Europhys. Lett. **38**, 183 (1997).

[16] A. Sarkar, J.-F. Leger, D. Chatenay, and J. F. Marko, Phys. Rev. E **63**, 051903 (2001).

[17] C. Storm and P. C. Nelson, Phys. Rev. E **67**, 051906 (2003).

[18] S. Cocco, J. Yan, J. F. Leger, D. Chatenay, and J. F. Marko, Phys. Rev. E **70**, 011910 (2004).

[19] J. Wenner, M. Williams, I. Rouzina, and V. Bloomfield, Biophys. J. **82**, 3160 (2002).

[20] L. Shokri, M. McCauley, I. Rouzina, and M. Williams, Biophys. J. **95**, 1248 (2008).

[21] J. van Mameren, P. Gross, G. Farge, P. Hooijman, M. Modesti, M. Falkenberg, G. J. L. Wuite, and E. J. G. Peterman, Proc. Natl. Acad. Sci. U.S.A. **106**, 18231 (2009).

[22] H. Fu, H. Chen, J. F. Marko, and J. Yan, Nucl. Acids Res. **38**, 5594 (2010).

[23] H. Fu, H. Chen, X. Zhang, J. F. Marko, and J. Yan, Nucl. Acids Res. **39**, 3473 (2011).

[24] N. Bosaeus, A. El-Sagheer, T. Brown, S. Smith, B. Akerman, C. Bustamante, and B. Nordén, Proc. Natl. Acad. Sci. U.S.A. **109**, 15179 (2012).

[25] G. A. King, P. Gross, U. Bockelmann, M. Modesti, G. J. L. Wuite, and E. J. G. Peterman, Proc. Natl. Acad. Sci. U.S.A. **110**, 3859 (2013).

[26] D. Paik and T. Perkins, J. Am. Chem. Soc. **133**, 3219 (2011).

[27] B. Essevaz-Roulet, U. Bockelmann, and F. Heslot, Proc. Natl. Acad. Sci. U.S.A. **94**, 11935 (1997).

[28] D. K. Lubensky and D. R. Nelson, Phys. Rev. E **65**, 031917 (2002).

[29] S. Cocco, R. Monasson, and J. F. Marko, Phys. Rev. E **66**, 051914 (2002).

[30] T. R. Strick, J.-F. Allemand, D. Bensimon, A. Bensimon, and V. Croquette, Science **271**, 1835 (1996).

[31] Z. Bryant, M. D. Stone, J. Gore, S. B. Smith, N. R. Cozzarelli, and C. Bustamante, Nature **424**, 338 (2003).

[32] S. Forth, C. Deufel, M. Y. Sheinin, B. Daniels, J. P. Sethna, and M. D. Wang, Phys. Rev. Lett. **100**, 148301 (2008).

[33] F. Mosconi, J.-F. Allemand, D. Bensimon, and V. Croquette, Phys. Rev. Lett. **102**, 078301 (2009).

[34] M. Y. Sheinin and M. D. Wang, Phys. Chem. Chem. Phys. **11**, 4800 (2009).

[35] J. Lipfert, J. W. Kerssemakers, T. Jager, and N. H. Dekker, Nat. Methods **7**, 977 (2010).

[36] M. Y. Sheinin, S. Forth, J. F. Marko, and M. D. Wang, Phys. Rev. Lett. **107**, 108102 (2011).

[37] F. C. Oberstrauss, L. E. Fernandes, and Z. Bryant, Proc. Natl. Acad. Sci. U.S.A. **109**, 6016 (2012).

[38] J.-F. Allemand, D. Bensimon, R. Lavery, and V. Croquette, Proc. Natl. Acad. Sci. U.S.A. **95**, 14152 (1998).

[39] J.-F. Leger, G. Romano, A. Sarkar, J. Robert, L. Bourdieu, D. Chatenay, and J. F. Marko, Phys. Rev. Lett. **83**, 1066 (1999).

[40] J. Schurr and B. Fujimoto, Biopolymers **99**, 1046 (2013).

[41] H. Zhang and J. F. Marko, Phys. Rev. E **77**, 031916 (2008).

[42] J. D. Moroz and P. Nelson, Proc. Natl. Acad. Sci. U.S.A. **94**, 14418 (1997).

[43] J. F. Marko, Phys. Rev. E **76**, 021926 (2007).

[44] A. E. H. Love, *A Treatise on the Mathematical Theory of Elasticity* (Dover, Mineola, NY, 1944).

[45] D. Stigter, J. Colloid Interface Sci. **53**, 296 (1975).

[46] W. Helfrich and W. Harbich, Chem. Src. **25**, 32 (1985).

[47] T. W. Burkhardt, J. Phys. A **30**, L167 (1997).

[48] A. Vologodskii, S. Levene, K. Klenin, M. Frank-Kamenetskii, and N. Cozzarelli, J. Mol. Biol. **227**, 1224 (1992).

[49] A. Vologodskii and N. Cozzarelli, Ann. Rev. Biophys. Biomol. Struct. **23**, 609 (1994).

[50] M.-N. Dessinges, B. Maier, Y. Zhang, M. Peliti, D. Bensimon, and V. Croquette, Phys. Rev. Lett. **89**, 248102 (2002).

[51] Y. Seol, G. M. Skinner, and K. Visscher, Phys. Rev. Lett. **93**, 118102 (2004).

[52] S. Cocco, J. F. Marko, R. Monasson, A. Sarkar, and J. Yan, Eur. Phys. J. E **10**, 249 (2003).

[53] N. M. Toan and D. Thirumalai, J. Chem. Phys. **136**, 235103 (2012).

[54] M. J. Stevens, D. McIntosh, and O. Saleh, Macromolecules **45**, 5757 (2012).

[55] J. F. Marko, Phys. Rev. E **55**, 1758 (1997).

[56] J. F. Marko, Phys. Rev. E **59**, 900 (1999).

[57] B. C. Daniels, S. Forth, M. Y. Sheinin, M. D. Wang, and J. P. Sethna, Phys. Rev. E **80**, 040901 (2009).

[58] H. Brutzer, N. Luzzietti, D. Klaue, and R. Seidel, Biophys. J. **98**, 1267 (2010).

[59] M. Emanuel, G. Lanzani, and H. Schiessel, Phys. Rev. E **88**, 022706 (2013).

[60] T. R. Strick, J.-F. Allemand, D. Bensimon, and V. Croquette, Biophys. J. **74**, 2016 (1998).

[61] A. Vologodskii and N. Cozzarelli, Biopolymers **35**, 289 (1995).

[62] D. Stigter and K. A. Dill, J. Phys. Chem. **97**, 12995 (1993).

[63] J. Ubbink and T. Odijk, Biophys. J. **76**, 2502 (1999).

[64] See Supplemental Material at http://link.aps.org/supplemental/10.1103/PhysRevE.88.062722 for values of the scaling parameter γ.